

ExoMol line lists – L: High-resolution line lists of H_3^+ , H_2D^+ , D_2H^+ and D_3^+ .

Charles A. Bowesman¹, Irina I. Mizus^{2,3}, Nikolay F. Zobov³, Oleg L. Polyansky^{1,3},
János Sarka^{4,5}, Bill Poirier⁴, Marco Pezzella¹, Sergei N. Yurchenko¹ and Jonathan Tennyson^{1*}

¹ *Department of Physics and Astronomy, University College London, Gower Street, WC1E 6BT London, UK;*

² *Holon Institute of Technology, Golomb Street, 52, Holon, 5810201, Israel;*

³ *Institute of Applied Physics, Russian Academy of Science, Ulyanov Street 46, Nizhniı Novgorod, Russia 603950;*

⁴ *Department of Chemistry and Biochemistry, Texas Tech University, Lubbock, Texas 79409, United States;*

⁵ *Institute of Chemistry, Eötvös Loránd University, Budapest, Hungary.*

8 June 2023

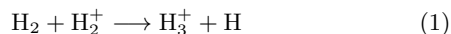
ABSTRACT

New MiZo line lists are presented for the D_2H^+ and D_3^+ isotopologues of H_3^+ . These line lists plus the existing H_3^+ MiZATeP and the Sochi H_2D^+ line lists are updated using empirical energy levels generated using the MARVEL procedure for H_3^+ , H_2D^+ and D_2H^+ , and effective Hamiltonian energies for D_3^+ for which there is significantly less laboratory data available. These updates allow accurate frequencies for far infrared lines for these species to be predicted. Assignments of the energy levels of H_3^+ and D_3^+ are extended using a combination of high accuracy variational calculations and analysis of transition intensities. All line lists are made available via www.exomol.com.

Key words: molecular data – opacity – planets and satellites: atmospheres – stars: atmospheres – ISM: molecules.

1 INTRODUCTION

H_3^+ is known to form rapidly in H_2 gas following an ionisation event via the strongly exothermic reaction



which occurs at essentially every collision. As H_2 is common in a variety of astronomical bodies, H_3^+ is often the dominant molecular ion. The first 30 years of H_3^+ astronomy has been comprehensively reviewed by Miller et al. (2020). H_3^+ formation is stimulated by cosmic ray ionisation of the interstellar medium and by collisions with fast electrons and other charged particles in planetary ionospheres. H_3^+ is also believed to form in the ionosphere of planets through the ionisation of H_2 by extreme ultraviolet radiation (Chadney et al. 2016). In gas giant ionospheres, H_3^+ acts as a coolant through efficient infrared (IR) emissions (Miller et al. 2010); indeed it is thought that H_3^+ emissions are key to determining the stability limits in hot Jupiter exoplanets (Koskinen et al. 2007).

The infrared spectrum of H_3^+ has been extensively observed in giant planets in our solar system such as Jupiter (Drossart et al. 1989; Ballester et al. 1994; Miller et al. 1997; Moore et al. 2017), Saturn (Geballe et al. 1993; Stallard et al. 2008a,b), Uranus (Trafton et al. 1993; Lam et al. 1997; Trafton et al. 1999; Melin et al. 2019) and is believed to be

present in Neptune (Melin et al. 2011, 2018) although it is yet to be detected there. Its presence can be used as an effective temperature probe here and in other astrophysical settings (Gibbs & Fitzgerald 2022). H_3^+ is similarly expected to be of importance in extrasolar giant planets (Chadney et al. 2016; Khodachenko et al. 2015), such as hot-Jupiters (Lenz et al. 2016), and an even more prominent feature in the aurorae of brown dwarfs (Gibbs & Fitzgerald 2022); however, it has so far defied observation on these objects.

H_3^+ has also been observed in the interstellar medium (ISM) via absorption in the infrared light of a background star (Oka 2006) where it forms through cosmic ray ionisation (Geballe & Oka 1996). Hence it is also used in this setting to trace the cosmic ray ionisation rate (Indriolo & McCall 2012; Harju et al. 2017) and similarly primarily relies on IR emissions. These IR bands lie well within the wavelength range of the instruments onboard the JWST.

In regions where the precursors to H_3^+ exist in deuterated forms, namely HD and D_2 , equivalent reactions occur to that described in Eq. (1) resulting in the formation of the deuterated isotopologues H_2D^+ , D_2H^+ and D_3^+ (Merkt et al. 2022). At low temperatures fractionation drives the preferential formation of isotopically substituted H_3^+ (Hewitt et al. 2005); indeed, models by Walmsley et al. (2004) suggest that in certain very cold regions D_3^+ may be the dominant isotopologue of H_3^+ ! Spectra of H_2D^+ (Stark et al. 1999; Caselli et al. 2003) and D_2H^+ (Vastel et al. 2004) have been observed in interstellar space through pure rotational transitions which lie in the

* The corresponding author: j.tennyson@ucl.ac.uk

far infrared / THZ region. However, D_3^+ remains undetected, at least in part because its higher symmetry means that, like H_3^+ , its pure rotational spectrum is very weak. Elsewhere, electrons provided by H_3^+ have been shown to play an important role in the atmospheres of cool white dwarfs (Bergeron et al. 1997).

Line lists for H_3^+ (Kao et al. 1991; Neale et al. 1996) and the associated partition function (Neale & Tennyson 1995; Ramanlal & Tennyson 2004) have played a key role in the astronomical study of this important molecular ion. In this work we update the MiZATeP H_3^+ line list of Mizus et al. (2017) and the older ST1 H_2D^+ line list of Sochi & Tennyson (2010). We do this using updated versions of the MARVEL (measured active rotation-vibration energy levels) studies due to Furtenbacher et al. (2013a) and Furtenbacher et al. (2013b). We present new line lists for D_2H^+ and D_3^+ , for which we also use empirical energy levels to improve the accuracy of the transition frequencies between key levels. These line lists are produced as part of the ExoMol project (Tennyson & Yurchenko 2012).

2 METHOD

The triatomic discrete variable representation (DVR) nuclear motion code DVR3D (Tennyson et al. 2004) was used previously and here to compute initial energy levels for H_3^+ and its deuterated isotopologues as well as Einstein A-coefficients for each transition. This code, which is based on the use of an exact nuclear motion kinetic energy operator, has been shown to be capable of giving highly accurate results for the H_3^+ system (Polyansky & Tennyson 1999; Pavanello et al. 2012a). It is important to note that in the absence of any absolute measurements of transition intensities for the H_3^+ system, all models rely on computed values which are thought to be accurate (Farnik et al. 2002; Petrigiani et al. 2014). It should be noted that DVR3D only provides assignments for the rigorous quantum numbers: J , rotationless parity e/f and the interchange symmetry for two identical atoms. This means that most states in the existing version of the MiZATeP H_3^+ (Mizus et al. 2017) and ST1 H_2D^+ (Sochi & Tennyson 2010) line lists do not have full ro-vibrational labels. We partially address this issue below.

MARVEL (Furtenbacher et al. 2007; Furtenbacher & Császár 2012; Tóbiás et al. 2018) takes assigned, high-resolution spectra and uses them to construct empirical energy levels with spectroscopic accuracy and specified uncertainties. Use of the energy levels can greatly improve the accuracy with which a line list can predict transition frequencies, see Al-Derzi et al. (2021) for a recent example. For H_3^+ , H_2D^+ and D_2H^+ MARVEL spectroscopic networks were then constructed using available laboratory spectra in order to obtain empirical energy levels for each species. These empirical energy levels were then used to improve our line lists, correcting for obs.–calc. shifts in levels where empirical energy levels are available for comparison. Such a refinement allows for a subset of the energies to be provided with very high accuracy, as has been demonstrated in similar projects (Bowesman et al. 2022). This allows for high-accuracy transition frequency predictions to be made (Al-Derzi et al. 2021), making the final line list well suited for high-resolution studies (Bowesman et al. 2021; Owens et al. 2022).

The MARVEL process determines an uncertainty for each energy level based on the uncertainties of the input transition that define that level.

2.1 Spectroscopic Networks

Transition data for a molecule can be aggregated to construct a spectroscopic network, where the transition frequencies represent the edges of the networks and the energy levels the nodes (Furtenbacher et al. 2007; Császár & Furtenbacher 2011). The MARVEL procedure (Furtenbacher & Császár 2012) achieves this by inverting transition matrices, which yields a set of empirical energy levels with individual uncertainties. Spectroscopic networks have been constructed in the past for the molecules H_3^+ (Furtenbacher et al. 2013a), H_2D^+ and D_2H^+ (Furtenbacher et al. 2013b) but new transition data has since been published. New transition data allows us to expand the level coverage of the networks and in the case of new data that remeasures existing transitions to improve the accuracy to which term energies are known. The recent high-resolution experiments have provided new THz transition data with uncertainties on the order of MHz or kHz, well within the part-per-billion regime. When all of the transitions that determine a level’s term energy are consistent within their experimental uncertainties, the uncertainty on the final term energy will generally be on the same order, but not less than, the smallest uncertainty of the transitions that define the level. Hence, with the addition of these high-accuracy transition measurements we are able to significantly improve the accuracy of our final energies, in some cases by a few orders of magnitude.

The MARVEL procedure requires all transitions within a network to be identified by the same set of quantum numbers. For this purpose, the deuterated isotopologues can be divided into two groups: H_3^+ and D_3^+ are symmetric-tops belonging to the $D_{3h}(M)$ molecular symmetry group and H_2D^+ and D_2H^+ are asymmetric-tops belonging to the $C_{2v}(M)$ group. These in turn dictate the set of good quantum numbers used to define the levels of the networks.

As symmetric tops, the molecules H_3^+ and D_3^+ are defined by two primary vibrational modes, symmetric stretching (ν_1) and bending (ν_2). The bending mode is degenerate however, and as such these species are also described by the vibrational angular momentum quantum number $l_2 = \nu_2, \nu_2 - 2, \dots, -\nu_2 + 2, -\nu_2$. The energy levels of these species are identified instead by $L_2 = |l_2|$ in this work. The rigorous rotational angular momentum quantum number J is used to define the rotational levels of these molecules. The projection of J along the molecular symmetry axis, k can be used to determine the parity of the energy levels, such that the total parity is the sign of $(-1)^k$ (Furtenbacher et al. 2013a). The quantum number k does not offer a complete description of the system however, due to Coriolis coupling between it and l_2 . As such, the value $G = |g|$ is used, where $g = k - l_2$ (Hougen 1962). This quantum number is important because, as members of the $D_{3h}(M)$ symmetry group, the A'_1, A''_1, A'_2, A''_2 rovibronic symmetries only exist for these molecules when $G = 3n$, where n is an integer. In H_3^+ the A'_1 and A''_1 symmetries do not exist however, as they are determined to have 0 nuclear spin statistical weight (Watson 1984). This difference arises from the nuclear spin I of constituent atoms, which are $I = \frac{1}{2}$ for hydrogen and $I = 1$ for deuterium. Consequently

Table 1. The rovibronic symmetries of the isotopologues of H_3^+ where g_{ns} is the nuclear spin statistical weight. For H_3^+ and D_3^+ ; Γ_{rve} are representations of the D_{3h} point group while for H_2D^+ and D_2H^+ they are for C_{2v} .

Γ_{rve}	Isomer	g_{ns}	Isomer	g_{ns}
	H_3^+		D_3^+	
A'_1, A''_1	-	0	ortho	10
A'_2, A''_2	ortho	4	para	1
E', E''	para	2	meta	8
	H_2D^+		D_2H^+	
A_1, A_2	para	3	ortho	12
B_1, B_2	ortho	9	para	6

H_3^+ consists of two nuclear spin isomers while D_3^+ has three (Watson et al. 1987); these are shown in Table 1.

Levels with equivalent vibrational, J and G assignments are differentiated by the $(u|l|m)$ U -notation of Watson (1994). u and l are used to identify the upper and lower energy levels of the same assignment, differing in their value of $K = |k|$, and m is used when such a distinction is irrelevant as only one value of K can exist that produces the same G . As such, the energy levels of the species H_3^+ and D_3^+ are identified by the quantum number set $(\nu_1, \nu_2, L_2, J, G, U, K, \Gamma_{\text{rve}})$.

As asymmetric-tops, H_2D^+ and D_2H^+ are defined by the symmetric stretching, bending and anti-symmetric stretching vibrational quantum numbers ν_1, ν_2 and ν_3 . The quantum number J and its projections onto the C_2 axis and the axis perpendicular to the C_2 axis in the plane of the molecule, K_a and K_c , are the standard ones for labelling the rotational states of an asymmetric top.

For both asymmetric-tops, the total parity is the sign of $(-1)^{K_c}$. A similar expression is used to identify the spin isomers of each asymmetric-top, such that they are labelled ortho when it is positive and para when negative. For H_2D^+ this is expression is $(-1)^{\nu_3+K_a}$ and for D_2H^+ it is $(-1)^{\nu_3+K_a+K_c}$. The ortho and para nuclear spin isomers identify the rovibronic symmetry group of the molecule, A_1, A_2, B_1 or B_2 , as shown in Table 1. Hence, the energy levels of the species H_2D^+ and D_2H^+ are identified by the quantum number set $(\nu_1, \nu_2, \nu_3, J, K_a, K_c, \Gamma_{\text{rve}})$.

Transitions between nuclear spin isomers are forbidden, meaning networks constructed from observational transitions will be split into separate components for each isomer. Given MARVEL determines the energies of each level relative to the lowest energy level in the network, which is defined as 0, this presents a problem as any levels of a different nuclear spin isomer to that of the zero-energy level will not have their energies defined. This is avoided by the introduction of “magic” numbers; forbidden transitions are added to the networks to connect the lowest levels of each nuclear spin isomer to each other using calculated energies. This enables the determination of all energies for connected levels within the networks, relative to the zero-energy level. For D_3^+ this treatment was not needed as the energies were determined through the use of effective Hamiltonian calculations.

2.1.1 H_3^+ network

Furtenbacher et al. (2013a) conducted a MARVEL study of H_3^+ which combined transition data from 26 sources into a single network. Since then, five new sets of high-accuracy spectra

have been reported (Berg et al. 2012; Hodges et al. 2013; Perry et al. 2015; Jusko et al. 2016; Guan et al. 2018; Markus & McCall 2019) and are detailed below:

12BeWoPe (Berg et al. 2012): 3 R-branch transitions in the visible region are provided that had not been included from other sources.

13HoPeJeSi (Hodges et al. 2013): 10 R-branch transitions in the ν_2 band with MHz and sub-MHz accuracy are reported. All of these transitions had been previously reported in other sources (Oka 1981; McKellar & Watson 1998) but are presented here at higher accuracy.

15PeHoMaKo (Perry et al. 2015): A further 10 R-branch transitions in the ν_2 band are reported with MHz and sub-MHz accuracy. All of the transitions from this source had been observed previously (Oka 1981; Lindsay et al. 2001; Wu et al. 2013).

16JuKoScAs (Jusko et al. 2016): 5 measurements of low- J R-branch transitions in the ν_2 band are provided, all with sub-MHz accuracy. These transitions had also been observed by *13HoPeJeSi* (Hodges et al. 2013).

18GuChLiPe (Guan et al. 2018): Transition frequencies for 12 R-branch and 4 Q-branch transitions in the ν_2 band are presented. The majority are reported with sub-MHz accuracy. All of the transitions in this source had also been observed in other experiments (Lindsay & McCall 2001; Hodges et al. 2013; Perry et al. 2015; Jusko et al. 2016; Perry et al. 2016).

19MaMc (Markus & McCall 2019): The largest of the new H_3^+ data sources, providing 36 measurements of transitions in the $\nu_2 \leftarrow 0$ band, 15 transitions in the $2\nu_2^2 \leftarrow \nu_2$ band and 7 transitions in the $2\nu_2^2 \leftarrow 0$ band. The data comprises a selection of P-, Q- and R-branch transitions with uncertainties of 4 MHz. All of the reported transitions had been observed in prior studies (Watson et al. 1984; Majewski et al. 1987; Bawendi et al. 1990; Xu et al. 1990; Uy et al. 1994; McKellar & Watson 1998; Guan et al. 2018; Markus et al. 2018).

In total there were 102 new transitions to be added to the existing set of 1610 transitions and a further 7 transitions that had been missed in the original MARVEL compilation. The inclusion of the new transitions allowed us to validate 19 previously invalidated transitions. 7 transitions had their assignment corrected based on updated assignments provided in subsequent papers. A further 9 transitions were reassigned based on apparent mixing identified through comparison with the empirical MARVEL energies. 2 transition assignments were updated based on suggestions provided by Jaquet (2022). Sarka & Poirier (2022) provided a series of assignments for H_3^+ which were used to correct the assignments of 41 transitions and to assign 22 previously unassigned transitions. A further three unassigned transitions from the literature were assigned based on comparison with the MARVEL energy levels. The new transition assignments are detailed in Table 2. The transitions updated in this way all involve levels with relatively high energies, in a region where accurate determination of the vibrational state can be challenging. In total, 59 transitions from the original network were reassigned and an additional 8 had their assignment corrected due to digitisation errors from the original source.

The final set of 1719 transitions were passed through MARVEL for validation, with 1656 being validated; these transitions are summarised in Table 3. The network is divided into 39 components, the largest of which comprises 1580 tran-

Table 2. The new transition assignments for transitions from the literature that previously had no assignment or were missing an upper state assignment. Assignments to transitions from [Lindsay et al. \(2001\)](#) were determined through comparison between the empirical energy levels determined by MARVEL, while transitions from [Morong et al. \(2009\)](#) were assigned based on assignments produced using the code ScallIT ([Sarka & Poirier 2022](#)).

Wavenumber (cm ⁻¹)	ν'_1	ν'_2	L'_2	J'	G'	U'	K'	Γ'_{rve}	ν''_1	ν''_2	L''_2	J''	G''	U''	K''	Γ''_{rve}	Source
3104.125(10)	2	0	0	6	1	m	1	E''	1	0	0	6	2	m	2	E'	Lindsay et al. (2001)
3182.605(5)	1	2	2	5	2	u	0	E'	0	2	0	5	1	m	1	E''	Lindsay et al. (2001)
3235.521(5)	1	2	2	7	5	u	3	E''	1	1	1	6	5	l	6	E'	Lindsay et al. (2001)
10329.307(10)	0	4	2	7	3	u	1	A'' ₂	0	0	0	6	6	m	6	A'' ₂	Morong et al. (2009)
10462.405(10)	0	5	1	5	6	m	5	A'' ₂	0	0	0	6	6	m	6	A'' ₂	Morong et al. (2009)
10496.287(10)	2	2	2	6	8	m	6	E'	0	0	0	5	5	m	5	E''	Morong et al. (2009)
10573.997(10)	0	4	4	5	0	m	4	A'' ₂	0	0	0	4	3	m	3	A'' ₂	Morong et al. (2009)
10639.058(10)	0	5	1	5	0	m	1	A'' ₂	0	0	0	5	0	m	5	A'' ₂	Morong et al. (2009)
10666.604(10)	0	5	1	5	3	l	4	A'' ₂	0	0	0	5	3	m	3	A'' ₂	Morong et al. (2009)
10827.764(10)	0	6	0	3	0	m	0	A'' ₂	0	1	1	2	0	m	1	A'' ₂	Morong et al. (2009)
11036.111(10)	0	5	1	7	6	l	7	A'' ₂	0	0	0	6	6	m	6	A'' ₂	Morong et al. (2009)
11046.569(10)	0	5	1	6	5	l	6	E'	0	0	0	5	5	m	5	E''	Morong et al. (2009)
11048.996(10)	0	5	1	5	4	l	5	E''	0	0	0	4	4	m	4	E'	Morong et al. (2009)
11114.628(10)	2	2	2	6	3	u	1	A'' ₂	0	0	0	5	0	m	5	A'' ₂	Morong et al. (2009)
11265.189(10)	1	5	3	3	0	m	3	A'' ₂	0	1	1	2	3	m	2	A'' ₂	Morong et al. (2009)
11331.112(10)	0	5	5	5	0	m	5	A'' ₂	0	0	0	6	6	m	6	A'' ₂	Morong et al. (2009)
11556.914(10)	0	5	3	5	3	m	0	A'' ₂	0	0	0	4	3	m	3	A'' ₂	Morong et al. (2009)
11947.074(10)	2	3	1	5	6	m	5	A'' ₂	0	0	0	6	6	m	6	A'' ₂	Morong et al. (2009)
12116.353(10)	0	6	0	3	3	m	3	A'' ₂	0	0	0	3	0	m	0	A'' ₂	Morong et al. (2009)
12331.180(10)	1	4	0	5	0	m	0	A'' ₂	0	0	0	4	3	m	3	A'' ₂	Morong et al. (2009)
12502.614(10)	0	6	2	2	0	m	2	A'' ₂	0	0	0	3	3	m	3	A'' ₂	Morong et al. (2009)
12536.621(10)	1	4	2	4	3	m	1	A'' ₂	0	0	0	3	0	m	0	A'' ₂	Morong et al. (2009)
13056.013(10)	0	6	2	2	3	m	1	A'' ₂	0	0	0	1	0	m	0	A'' ₂	Morong et al. (2009)
13597.367(10)	0	6	4	1	3	m	1	A'' ₂	0	0	0	1	0	m	0	A'' ₂	Morong et al. (2009)
13676.446(10)	0	7	1	1	0	m	1	A'' ₂	0	0	0	1	0	m	0	A'' ₂	Morong et al. (2009)

sitions which determine 703 empirical energy levels. Of the remaining components: two consist of 6 transitions; one of 5 transitions; two of 4 transitions; three of 3 transitions; 12 of 2 transitions and the remaining 18 of single transitions. As these minor components are not connected to the primary component the energies of the levels within them are not determined relative to the zero-energy level and are hence not considered further.

2.1.2 H₂D⁺ network

A MARVEL network for H₂D⁺ was originally produced by [Furtenbacher et al. \(2013b\)](#) and contained transition data from 13 sources. Since then, two new sets of transition measurements have been published by [Jusko et al. \(2016\)](#) and [Jusko et al. \(2017\)](#).

16JuKoScAs ([Jusko et al. 2016](#)): Transitions frequencies for 11 ν_1 band transitions are reported with MHz and sub-MHz accuracy. This source provides significantly higher accuracy measurements of transitions previously observed by [Amano \(1985\)](#).

17JuToMuGh ([Jusko et al. 2017](#)): 3 pure-rotation transition measurements are provided with sub-MHz or kHz accuracy.

These two new sources and a “magic” forbidden transition to connect the nuclear spin isomers, derived from effective Hamiltonian calculations using molecular constants from [Amano \(2006\)](#), brought the total number of transitions for H₂D⁺ to 210; these are summarised in [Table 4](#). 208 transitions were validated successfully by MARVEL, yielding a final network comprising 7 components, the largest of which contained 200 transitions that determine 109 unique energy levels. For the remaining 6 components, one contained 3 tran-

sitions while the rest are single transition components; these disconnected components are not considered further here.

2.1.3 D₂H⁺ network

The D₂H⁺ MARVEL network was originally published by [Furtenbacher et al. \(2013b\)](#) and was constructed using transition data from 9 sources. Four new sets of transition data have subsequently been published ([Jusko et al. 2016, 2017](#); [Yu. et al. 2017](#); [Markus et al. 2019](#)) and have now been added to the existing network.

16JuKoScAs ([Jusko et al. 2016](#)): This source provides 10 transitions frequencies observed with sub-MHz accuracy. 8 of these transitions had been previously observed by [Lubic & Amano \(1984\)](#).

17JuToMuGh ([Jusko et al. 2017](#)): 3 ground state pure-rotation transition measurements are provided with kHz accuracy.

17YuPeAmMa ([Yu. et al. 2017](#)): This source reports 5 ground state pure-rotation transitions with sub-MHz accuracy. 4 of these transitions had not been reported in other sources, with the other also being observed by [Jusko et al. \(2017\)](#).

19MaKoMc ([Markus et al. 2019](#)): Transition frequencies for 37 ν_1 band transitions are provided with MHz accuracy. 10 of the transitions in this source are new and had not been reported elsewhere, while the rest had been observed by [Lubic & Amano \(1984\)](#) and [Jusko et al. \(2016\)](#).

With the addition of 55 new transition measurements, the new network contains 210 transitions. Two existing transitions that had digitisation errors in their transitions frequencies were updated to the correct values. A “magic” forbidden transition is included to connect the otherwise distinct ortho and para components of the network, using an frequency cal-

Table 3. The components of the updated H_3^+ MARVEL network. The network is broken down by the transition data sources and the vibrational bands contained within them, given in the form $\nu'_1, \nu'_2, L'_2 - \nu''_1, \nu''_2, L''_2$. For each band, the transition energy and total angular momentum J ranges are provided, along with the mean and maximum uncertainties for these transitions. The total number of transitions validated and accessed by MARVEL (V/A) are also provided.

Vib.	J range	V/A	Energy range (cm^{-1})	Uncertainty Mean/Max (cm^{-1})
80Oka (Oka 1980)				
011 - 000	0 - 4	14/15	2457 - 2918	0.013/0.015
81Oka (Oka 1981)				
011 - 000	0 - 6	27/30	2457 - 3030	0.010/0.010
84WaFoMcBe (Watson et al. 1984)				
011 - 000	0 - 7	46/46	2217 - 3030	0.010/0.010
84WaFoMcBe_CD (Watson et al. 1984)				
000 - 000	1 - 4	5/5	173 - 596	0.010/0.012
87MaMaMcJo (Majewski et al. 1987)				
011 - 000	0 - 10	110/113	1798 - 3193	0.010/0.020
89MaFeWaMi (Majewski et al. 1989)				
022 - 000	1 - 12	44/50	4540 - 5094	0.017/0.041
90BaReOk (Bawendi et al. 1990)				
011 - 000	3 - 9	14/14	2468 - 2889	0.010/0.010
020 - 011	1 - 6	14/14	2395 - 2685	0.010/0.010
022 - 011	0 - 8	68/68	2090 - 2945	0.010/0.040
111 - 011	5 - 6	2/2	2741 - 2854	0.010/0.010
111 - 100	1 - 4	21/21	2089 - 2771	0.010/0.010
90NaItSuTa (Nakanaga et al. 1990)				
011 - 000	0 - 3	11/12	2457 - 2762	0.010/0.010
90XuGaOk (Xu et al. 1990)				
022 - 000	1 - 10	34/34	4557 - 5094	0.011/0.040
91LeVeCaOk (Lee et al. 1991)				
031 - 000	1 - 5	3/4	6866 - 6878	0.012/0.017
92XuRoGaOk (Xu et al. 1992)				
011 - 000	5 - 13	30/30	2419 - 3291	0.010/0.014
022 - 011	3 - 7	9/10	2893 - 3215	0.010/0.010
022 - 100	6 - 7	1/1	2980 - 2980	0.010/0.010
100 - 000	4 - 7	9/9	2454 - 3282	0.010/0.010
111 - 011	0 - 6	21/21	2437 - 3229	0.010/0.010
120 - 022	4 - 5	1/1	2990 - 2990	0.010/0.010
211 - 111	2 - 3	1/1	3006 - 3006	0.010/0.010
94MaMcSaWa (Majewski et al. 1994)				
011 - 000	5 - 14	67/67	1844 - 3643	0.014/0.050
020 - 011	1 - 10	27/27	1934 - 3024	0.013/0.050
022 - 000	2 - 8	9/11	4435 - 4795	0.017/0.030
022 - 011	1 - 10	57/63	1869 - 3293	0.013/0.040
022 - 100	5 - 6	1/2	2836 - 2836	0.010/0.010
031 - 011	n/a	0/1	nan - nan	nan/nan
031 - 020	1 - 7	2/2	2260 - 3002	0.010/0.010
033 - 011	3 - 4	2/2	4553 - 4721	0.020/0.030
033 - 022	3 - 7	3/4	2028 - 3241	0.010/0.010
100 - 000	7 - 11	4/4	3024 - 3277	0.010/0.010
111 - 000	6 - 7	1/1	4949 - 4949	0.040/0.040
111 - 011	1 - 9	13/18	2766 - 3288	0.067/0.707
111 - 100	2 - 11	36/38	1928 - 3204	0.011/0.042
120 - 022	6 - 7	1/1	3206 - 3206	0.010/0.010
122 - 020	9 - 10	1/1	2943 - 2943	0.010/0.010
122 - 022	n/a	0/1	nan - nan	nan/nan
94UyGaJaOk (Uy et al. 1994)				
011 - 000	1 - 16	73/73	2691 - 3579	0.011/0.040
100 - 000	8 - 10	2/2	3412 - 3441	0.010/0.010
94VeCaGuJo (Ventrudo et al. 1994)				
031 - 000	1 - 5	14/15	6807 - 7266	0.017/0.040
97DiNePoTe (Dinelli et al. 1997)				
000 - 020	n/a	0/1	nan - nan	nan/nan
011 - 000	6 - 14	14/16	2396 - 3269	0.012/0.040
020 - 011	4 - 10	9/10	2622 - 2998	0.013/0.040
020 - 100	9 - 10	1/1	2893 - 2893	0.010/0.010
022 - 011	4 - 13	17/24	2413 - 3240	0.010/0.010
022 - 100	4 - 6	2/4	2571 - 2709	0.010/0.010
031 - 020	1 - 9	9/9	2458 - 2977	0.010/0.010
031 - 022	4 - 6	2/2	2680 - 2709	0.010/0.010

Table 3 - continued.

Vib.	J range	V/A	Energy range (cm^{-1})	Uncertainty Mean/Max (cm^{-1})
97DiNePoTe (Dinelli et al. 1997)				
033 - 022	0 - 9	19/20	2484 - 3061	0.010/0.010
100 - 000	8 - 8	1/1	2471 - 2471	0.010/0.010
111 - 011	4 - 7	5/9	2661 - 3203	0.020/0.030
111 - 100	4 - 11	7/7	2458 - 3294	0.013/0.030
120 - 022	2 - 6	2/2	2852 - 3052	0.010/0.010
120 - 111	4 - 6	2/2	2714 - 2817	0.025/0.040
122 - 111	2 - 7	7/7	2403 - 3022	0.010/0.010
211 - 200	1 - 6	3/3	2416 - 2654	0.010/0.010
00McOk (McCall & Oka 2000)				
120 - 000	3 - 4	1/1	8038 - 8038	0.010/0.010
122 - 000	1 - 5	27/27	7785 - 8163	0.014/0.040
211 - 000	4 - 6	2/2	8053 - 8123	0.010/0.010
01LiMc (Lindsay & McCall 2001)				
011 - 000	6 - 7	1/1	2956 - 2956	0.010/0.010
020 - 011	7 - 10	3/3	2902 - 2977	0.017/0.030
020 - 100	8 - 9	1/1	3003 - 3003	0.010/0.010
022 - 011	3 - 8	4/4	2601 - 2953	0.015/0.020
022 - 100	5 - 7	3/3	2844 - 2980	0.010/0.010
031 - 020	3 - 7	2/2	2596 - 2716	0.010/0.010
033 - 022	0 - 5	4/4	2469 - 2579	0.010/0.010
100 - 000	7 - 8	1/1	2957 - 2957	0.030/0.030
111 - 011	5 - 9	9/9	2437 - 3000	0.010/0.010
111 - 100	1 - 9	4/4	2575 - 2902	0.010/0.010
120 - 022	4 - 6	2/2	2976 - 2990	0.010/0.010
120 - 111	5 - 6	1/1	2817 - 2817	0.010/0.010
122 - 111	1 - 6	8/8	2497 - 2893	0.015/0.030
211 - 111	4 - 6	2/2	2891 - 2903	0.010/0.010
211 - 200	5 - 6	1/1	2654 - 2654	0.010/0.010
01LiMc.MAGIC (Lindsay & McCall 2001)				
000 - 000	0 - 1	3/3	22.839 - 86.960	$1.00 \times 10^{-9} / 1.00 \times 10^{-9}$
01LiRaOk (Lindsay et al. 2001)				
011 - 000	4 - 16	96/96	3008 - 3596	0.008/0.045
020 - 011	8 - 13	6/6	2998 - 3283	0.007/0.015
020 - 100	9 - 10	1/1	3111 - 3111	0.010/0.010
022 - 011	4 - 12	75/75	3007 - 3527	0.007/0.040
022 - 100	7 - 9	4/4	3101 - 3269	0.013/0.035
031 - 020	5 - 8	2/2	3003 - 3134	0.005/0.005
033 - 022	5 - 6	1/1	3076 - 3076	0.010/0.010
100 - 000	4 - 11	22/22	3024 - 3575	0.009/0.045
111 - 011	0 - 9	24/25	3009 - 3443	0.006/0.015
111 - 100	6 - 10	14/14	3024 - 3296	0.006/0.010
120 - 020	6 - 7	1/1	3063 - 3063	0.015/0.015
120 - 022	5 - 6	2/2	3018 - 3052	0.005/0.005
122 - 020	5 - 5	1/1	3183 - 3183	0.005/0.005
122 - 111	6 - 7	2/2	3022 - 3236	0.005/0.005
200 - 100	6 - 8	3/3	3077 - 3104	0.008/0.010
03GoMcOk (Gottfried et al. 2003)				
051 - 000	1 - 4	7/7	11019 - 11576	0.011/0.015
053 - 000	1 - 3	2/2	11044 - 11247	0.010/0.010
055 - 000	1 - 3	5/5	11572 - 11854	0.010/0.010
062 - 000	1 - 1	1/1	12419 - 12419	0.010/0.010
142 - 000	1 - 2	1/1	12246 - 12246	0.020/0.020
231 - 000	1 - 3	3/3	12222 - 12254	0.013/0.020
311 - 000	1 - 3	3/3	11112 - 11504	0.010/0.010
04MiKrWePl (Mikosch et al. 2004)				
031 - 000	1 - 3	3/3	7193 - 7241	0.015/0.026
04OkEp (Oka & Epp 2004)				
011 - 000	1 - 7	20/20	2530 - 3182	0.011/0.020
022 - 000	1 - 7	10/11	4777 - 4987	0.015/0.054
04OkEp_CD (Oka & Epp 2004)				
000 - 000	1 - 10	68/69	7.255 - 1696	0.011/0.022
08KrBiRePe (Kreckel et al. 2008)				
051 - 000	1 - 2	2/2	11229 - 11244	0.010/0.010
055 - 000	0 - 2	4/4	11594 - 11882	0.010/0.010
062 - 000	1 - 2	5/5	12419 - 13072	0.011/0.014
142 - 000	1 - 2	2/2	12019 - 12087	0.010/0.010
144 - 000	1 - 2	1/1	12898 - 12898	0.010/0.010
231 - 000	0 - 1	1/1	12239 - 12239	0.010/0.010
311 - 000	0 - 2	4/4	11259 - 11511	0.010/0.010
322 - 000	1 - 2	1/1	13333 - 13333	0.010/0.010

Table 3 - continued.

Vib.	J range	V/A	Energy range (cm^{-1})	Uncertainty Mean/Max (cm^{-1})
08VeLeAgBe (Velilla et al. 2008)				
051 - 000	1 - 3	4/4	10730 - 10790	0.010/0.010
062 - 000	1 - 3	2/2	12503 - 13056	0.010/0.010
142 - 000	3 - 4	1/1	12658 - 12658	0.010/0.010
144 - 000	1 - 2	1/1	12898 - 12898	0.010/0.010
222 - 000	1 - 3	4/4	10726 - 10779	0.010/0.010
09MoGoOk (Morong et al. 2009)				
042 - 000	6 - 7	1/1	10329 - 10329	0.010/0.010
044 - 000	2 - 5	4/4	10367 - 10574	0.010/0.010
051 - 000	0 - 7	38/39	10462 - 11619	0.010/0.015
053 - 000	1 - 5	9/9	10657 - 11954	0.010/0.010
055 - 000	1 - 6	19/19	11331 - 12321	0.010/0.010
060 - 000	3 - 3	1/1	12116 - 12116	0.010/0.010
060 - 011	2 - 3	1/1	10828 - 10828	0.010/0.010
062 - 000	1 - 3	4/4	12419 - 13056	0.014/0.025
064 - 000	1 - 1	1/1	13597 - 13597	0.010/0.010
071 - 000	1 - 1	1/1	13676 - 13676	0.010/0.010
140 - 000	3 - 5	3/3	11563 - 12331	0.010/0.010
142 - 000	1 - 4	5/5	12102 - 12658	0.010/0.010
144 - 000	1 - 2	1/1	12898 - 12898	0.010/0.010
153 - 011	2 - 3	1/1	11265 - 11265	0.010/0.010
220 - 000	4 - 5	1/1	11114 - 11114	0.010/0.010
222 - 000	0 - 6	32/33	10322 - 11115	0.010/0.010
231 - 000	1 - 6	7/7	11947 - 12525	0.011/0.020
311 - 000	1 - 6	11/11	10875 - 11892	0.010/0.010
12BeWoPe (Berg et al. 2012)				
144 - 000	1 - 2	1/1	12882 - 12882	0.005/0.005
231 - 000	1 - 2	1/1	12589 - 12589	0.005/0.005
233 - 000	1 - 2	1/1	12620 - 12620	0.005/0.005
12CrHoSiPe (Crabtree et al. 2012)				
011 - 000	1 - 2	1/1	2726 - 2726	0.004/0.004
12PaAdAlZo (Pavanello et al. 2012a)				
051 - 000	0 - 1	2/2	10799 - 10832	0.005/0.005
062 - 000	0 - 1	1/1	12413 - 12413	0.010/0.010
071 - 000	0 - 1	1/1	13638 - 13638	0.005/0.005
082 - 000	0 - 1	1/1	15059 - 15059	0.005/0.005
162 - 000	1 - 2	2/2	15130 - 15450	0.005/0.005
164 - 000	1 - 2	1/1	15643 - 15643	0.005/0.005
222 - 000	1 - 2	1/1	10752 - 10752	0.005/0.005
231 - 000	1 - 2	3/3	12374 - 12589	0.008/0.010
233 - 000	1 - 2	1/1	12620 - 12620	0.005/0.005
251 - 000	1 - 1	1/1	15717 - 15717	0.005/0.005
342 - 000	1 - 2	1/1	16506 - 16506	0.005/0.005
13HoPeJeSi (Hodges et al. 2013)				
011 - 000	1 - 5	10/10	2691 - 2894	$2.40 \times 10^{-5}/4.51 \times 10^{-5}$
13WuLiLiSh (Wu et al. 2013)				
011 - 000	1 - 4	12/12	2518 - 2918	$3.14 \times 10^{-4}/1.00 \times 10^{-3}$
15PeHoMaKo (Perry et al. 2015)				
011 - 000	3 - 7	10/10	2895 - 3030	$6.93 \times 10^{-5}/1.30 \times 10^{-4}$
16JuKoScAs (Jusko et al. 2016)				
011 - 000	1 - 3	5/5	2691 - 2823	$1.08 \times 10^{-5}/2.20 \times 10^{-5}$
18GuChLiPe (Guan et al. 2018)				
011 - 000	1 - 6	16/16	2530 - 3015	$5.20 \times 10^{-5}/3.00 \times 10^{-4}$
19MaMc (Markus & McCall 2019)				
011 - 000	0 - 6	36/36	2217 - 3008	$1.67 \times 10^{-4}/6.33 \times 10^{-4}$
022 - 000	1 - 4	7/7	4968 - 5094	$2.16 \times 10^{-4}/6.45 \times 10^{-4}$
022 - 011	0 - 5	15/15	2474 - 2945	$1.48 \times 10^{-4}/2.16 \times 10^{-4}$

culated by Yu. et al. (2017). The final set of D_2H^+ transition data is summarised in Table 5. All of the transitions in the network were validated by MARVEL, yielding a primary network component containing 200 transitions which define 115 unique energy levels. The rest of the transitions are present in 7 disconnected components, one of which contains 3 transitions, another 2 transitions and the remainder are single transition components.

Table 4. The components of the updated H_2D^+ MARVEL network. The network is broken down by the transition data sources and the vibrational bands contained within them, given in the form $\nu'_1, \nu'_2, \nu'_3 - \nu''_1, \nu''_2, \nu''_3$. For each band, the transition energy and total angular momentum J ranges are provided, along with the mean and maximum uncertainties for these transitions. The total number of transitions validated and accessed by MARVEL (V/A) are also provided.

Vib.	J range	V/A	Energy range (cm^{-1})	Uncertainty Mean/Max (cm^{-1})
84AmWa (Amano & Watson 1984)				
100 - 000	0 - 5	26/27	2841 - 3179	0.002/0.004
84BoDeDeDe (Bogey et al. 1984)				
000 - 000	1 - 1	1/1	12.423 - 12.423	$6.67 \times 10^{-6}/6.67 \times 10^{-6}$
84WaCoPeWo (Warner et al. 1984)				
000 - 000	1 - 1	1/1	12.423 - 12.423	$3.34 \times 10^{-6}/3.34 \times 10^{-6}$
85Amano (Amano 1985)				
100 - 000	0 - 5	37/37	2839 - 3208	0.006/0.040
85SaKaHi (Saito et al. 1985)				
000 - 000	2 - 2	1/1	5.2032 - 5.2032	$1.23 \times 10^{-6}/1.23 \times 10^{-6}$
86FoMcPeWa (Foster et al. 1986a)				
001 - 000	0 - 5	42/42	2109 - 2602	0.006/0.042
010 - 000	0 - 7	31/31	1838 - 2537	0.004/0.005
02FaDaKo (Farnik et al. 2002)				
002 - 000	1 - 2	1/1	4538 - 4538	0.002/0.002
011 - 000	0 - 2	3/3	4423 - 4513	$8.67 \times 10^{-4}/0.001$
020 - 000	1 - 2	4/4	4271 - 4394	0.001/0.002
05AmHi (Amano & Hirao 2005)				
000 - 000	1 - 3	2/3	12.423 - 21.563	$1.31 \times 10^{-6}/1.67 \times 10^{-6}$
06Amano (Amano 2006)				
000 - 000	1 - 3	3/3	85.9513 - 115	$2.72 \times 10^{-5}/3.34 \times 10^{-5}$
06Amano.MAGIC (Amano 2006)				
000 - 000	0 - 1	1/1	60.030 - 60.030	$1.00 \times 10^{-5}/1.00 \times 10^{-5}$
06HIKOPiKO (Hlavenka et al. 2006a)				
021 - 000	0 - 2	3/3	6459 - 6491	0.021/0.031
07AsHuMuKu (Asvany et al. 2007)				
021 - 000	0 - 3	9/9	6341 - 6589	0.002/0.002
030 - 000	0 - 1	4/4	6242 - 6331	0.002/0.002
100 - 000	0 - 2	5/5	2947 - 3164	0.004/0.005
120 - 000	0 - 2	7/7	6946 - 7106	0.002/0.002
08AsRiMuWi (Asvany et al. 2008)				
000 - 000	0 - 1	1/1	45.701 - 45.701	$6.67 \times 10^{-7}/6.67 \times 10^{-7}$
09YoMaMoTa (Yonezu et al. 2009)				
000 - 000	0 - 3	8/8	5.2032 - 115	$3.27 \times 10^{-5}/2.01 \times 10^{-4}$
16JuKoScAs (Jusko et al. 2016)				
100 - 000	0 - 2	11/11	2887 - 3095	$2.66 \times 10^{-5}/1.50 \times 10^{-4}$
16JuKoScAs.CD (Jusko et al. 2016)				
000 - 000	0 - 2	4/4	66.4066 - 132	$6.75 \times 10^{-5}/1.51 \times 10^{-4}$
17JuToMuGh (Jusko et al. 2017)				
000 - 000	0 - 2	3/3	12.423 - 45.701	$1.19 \times 10^{-6}/3.07 \times 10^{-6}$

2.2 Effective Hamiltonians

There have been significantly fewer observations of D_3^+ spectra than of the three other isotopologues considered here. As such, there was insufficient data to build a well-connected network. In lieu of this, we used effective Hamiltonian constants from Watson et al. (1987) and Amano et al. (1994) to calculate energies for the states in the range $J = 0 - 15$, up to a maximum energy of 2676.387 cm^{-1} . These calculations were performed using the program PGOPHER (Western 2017) which also provides full state assignments for the levels it computes. Hence full quantum number assignments were determined via this method for 282 levels within the bands for which constants were available: 188 levels in the 000 band (ν_1, ν_2, L_2); 2 levels in the 010 band; 105 in the 011 band; 22 in the 100 band. The majority of the levels assigned through this method have $J < 10$. Further assignments were done manually for states at higher energies with the aid of the

Table 5. The components of the updated D_2H^+ MARVEL network. The network is broken down by the transition data sources and the vibrational bands contained within them, given in the form $\nu'_1, \nu'_2, \nu'_3 - \nu''_1, \nu''_2, \nu''_3$. For each band, the transition energy and total angular momentum J ranges are provided, along with the mean and maximum uncertainties for these transitions. The total number of transitions validated and accessed by MARVEL (V/A) are also provided.

Vib.	J range	V/A	Energy range (cm $^{-1}$)	Uncertainty Mean/Max (cm $^{-1}$)
84LuAm (Lubic & Amano 1984)				
100 - 000	0 - 6	34/34	2638 - 2990	0.005/0.005
86FoMcWa (Foster et al. 1986b)				
001 - 000	0 - 5	35/35	1916 - 2291	0.005/0.005
010 - 000	0 - 6	53/53	1782 - 2280	0.004/0.005
90PoMc (Polyansky & McKellar 1990)				
010 - 000	3 - 4	1/1	2276 - 2276	0.005/0.005
02FaDaKoPo (Farnik et al. 2002)				
002 - 000	0 - 2	6/6	3994 - 4066	$6.17 \times 10^{-4} / 9.00 \times 10^{-4}$
011 - 000	0 - 2	6/6	3983 - 4122	0.002/0.004
020 - 000	0 - 2	4/4	3847 - 3887	0.003/0.004
03HiAm (Hirao & Amano 2003)				
000 - 000	1 - 1	1/1	23.071 - 23.071	$6.00 \times 10^{-7} / 6.00 \times 10^{-7}$
05AmHi (Amano & Hirao 2005)				
000 - 000	0 - 2	3/3	23.071 - 49.254	$1.00 \times 10^{-5} / 1.00 \times 10^{-5}$
06HIPiBa (Hlavenka et al. 2006b)				
102 - 000	0 - 3	3/3	6534 - 6536	0.005/0.005
07AsHuMuKu (Asvany et al. 2007)				
102 - 000	0 - 2	5/5	6467 - 6536	0.005/0.005
111 - 000	0 - 1	1/1	6581 - 6581	0.005/0.005
120 - 000	0 - 1	1/1	6482 - 6482	0.005/0.005
08AsRiMuWi (Asvany et al. 2008)				
000 - 000	0 - 1	1/1	49.254 - 49.254	$5.00 \times 10^{-7} / 5.00 \times 10^{-7}$
16JuKoScAs (Jusko et al. 2016)				
100 - 000	0 - 2	10/10	2684 - 2866	$8.80 \times 10^{-6} / 2.60 \times 10^{-5}$
17JuToMuGh (Jusko et al. 2017)				
000 - 000	0 - 2	3/3	23.071 - 49.254	$2.08 \times 10^{-7} / 3.34 \times 10^{-7}$
17YuPeAmMa (Yu. et al. 2017)				
000 - 000	1 - 3	5/5	34.646 - 98.311	$3.34 \times 10^{-6} / 3.34 \times 10^{-6}$
17YuPeAmMa_MAGIC (Yu. et al. 2017)				
000 - 000	0 - 1	1/1	34.918 - 34.918	$1.00 \times 10^{-5} / 1.00 \times 10^{-5}$
19MaKoMc (Markus et al. 2019)				
100 - 000	0 - 5	37/37	2588 - 2928	$6.83 \times 10^{-5} / 1.15 \times 10^{-4}$

vibrational band origins published by Amano et al. (1994) and the assigned hot and overtone bands published by Al-ijah et al. (1995). A further 1045 states were assigned this way and a breakdown of the assigned bands is given in Table 6. These assignments were added to the calculated states file, given that DVR3D only provides assignments for the rigorous quantum numbers: J , rotationless parity e/f and interchange of two of the D atoms.

3 LINE LIST CALCULATIONS

3.1 Updated H_3^+ and H_2D^+

While the main line lists were computed using DVR3D, we took advantage of calculations by Sarka et al. (2021); Sarka & Poirier (2022) performed using the variational nuclear motion programs SCALIT (Chen & Poirier 2006a,b, 2010b,a; Petty & Poirier 2014), and GENIUSH (Mátyus et al. 2009; Fábri et al. 2011) to give full quantum number designations. The approach applied is detailed by Sarka & Poirier (2022) but we provide a quick summary of the main steps here. First, using Jacobi coordinates SCALIT calculations were carried out in the four blocks of the G_4 permutation-inversion (PI)

Table 6. The assigned vibrational bands of the D_3^+ states file, detailing the J range and maximum energy of each band.

ν_1	ν_2	L_2	Count	Energy range (cm $^{-1}$)	J range
0	0	0	256	0 - 4753	0 - 15
0	1	1	380	1835 - 6300	0 - 15
0	2	0	99	3531 - 6830	0 - 15
0	2	2	253	3646 - 7551	0 - 15
0	3	1	11	5214 - 5513	0 - 3
0	3	3	6	5401 - 5513	0 - 1
0	4	0	1	6774	0
0	4	2	2	6860 - 6860	0
0	4	4	2	7170 - 7170	0
0	5	1	2	8298 - 8298	0
0	5	3	2	8376 - 8600	0
0	5	5	2	8791 - 8791	0
0	6	0	1	9696	0
0	6	2	2	9731 - 9731	0
1	0	0	140	2301 - 5436	0 - 15
1	1	1	99	4060 - 7800	0 - 14
1	2	0	4	5712 - 5756	0 - 1
1	2	2	4	5796 - 6169	0 - 4
1	3	1	2	7368 - 7368	0
1	3	3	2	7454 - 7536	0
1	4	0	1	8864	0
1	4	2	2	9031 - 9031	0
1	4	4	2	9163 - 9163	0
2	0	0	36	4555 - 5178	0 - 5
2	1	1	2	6237 - 6237	0
2	2	0	1	7831	0
2	2	2	2	7894 - 7894	0
2	3	1	2	9424 - 9424	0
2	3	3	2	9463 - 9555	0
3	0	0	1	6761	0
3	1	1	2	8366 - 8366	0
3	2	0	1	9896	0
3	2	2	2	9943 - 9943	0
4	0	0	1	8921	0

symmetry group. Due to the very high convergence accuracy, the full G_{12} PI group labels (Γ_{rve}) were easily assigned unambiguously using the $\Gamma(G_{12}/D_{3h}) \downarrow G_4$ correlation table. Next, calculations were repeated with the code GENIUSH with slightly lower accuracy, but still sufficient to match the energy levels with the SCALIT ones. After the vibrational states were labelled (ν_1, ν_2, L_2), vibrational parent labels were semi-automatically assigned to rovibrational states using the rigid rotor decomposition scheme (RRD) implemented in GENIUSH (Mátyus et al. 2010). The RRD overlaps of GENIUSH also help to assign the rotational quantum numbers (J, G, U, K), as the symmetric top rigid rotor functions are labelled by K . Using this method we were able to label by the quantum number set ($\nu_1, \nu_2, L_2, J, G, U, K, \Gamma_{rve}$) an additional 1525 states in the MiZATeP H_3^+ line list.

The energies of the existing H_3^+ and H_2D^+ line lists were updated with empirical energies where they were known. For levels with matching assignments in both the states files and corresponding MARVEL network, the term energies and their uncertainties were set to the values determined by the MARVEL procedure. For the levels that did not exist within the molecules' MARVEL network, the calculated term energies were retained and estimates for their uncertainties were

calculated as follows

$$\Delta\tilde{E} = \begin{cases} 0.1, & \text{if } \tilde{E} < 2000 \\ \lfloor \tilde{E}/2000 \rfloor / 10, & \text{otherwise.} \end{cases} \quad (2)$$

3.2 New line lists

New line lists were computed for D_2H^+ and D_3^+ molecular ions. Both calculations used the highly accurate global *ab initio* PES, together with adiabatic and relativistic correction surfaces, computed by Pavanello et al. (2012a,b) which were used for the MiZATeP line list. To calculate transitions intensities the high-accuracy DMS obtained for the H_3^+ system was used (Petrigani et al. 2014). This DMS was obtained by fitting 7 parameters to a polynomial form written in terms of effective charges, see Röhse et al. (1994). This DMS was centred on the centre-of-mass ensuring the correct treatment of the centre-of-charge – centre-of-mass displacement which leads to D_2H^+ (and H_2D^+) having a permanent dipole moment.

The DVR3D program suite (Tennyson et al. 2004) was used to compute the final line lists. As part of this project a new module was added to this suite which converts DVR3D results to ExoMol format (Tennyson et al. 2013) comprising a states and trans file, and allowing spectra to be easily generated using EXOCROSS (Yurchenko et al. 2018). The module reads the energy levels and Einstein coefficients from DVR3D, requiring as input from the user the molecular symmetry, C_s or C_{2v} , and the nuclear statistic weight for each symmetry. The program, called LINELIST, is available as part of the DVR3D program suite from the ExoMol GitHub pages.

As with H_3^+ and H_2D^+ , the calculated term energies of D_2H^+ were updated with empirical values from the new MARVEL network where available. Likewise, the unchanged calculated energies of the new D_2H^+ and D_3^+ line lists had uncertainties estimated using Eq. (2).

3.3 D_2H^+ nuclear motion calculations

DVR3D nuclear motion calculations were performed in the following way: with 31, 31, and 50 grid points for two radial and an angular scattering coordinates. The calculations used Morse-like oscillators with parameters 3.1, 0.1, and 0.006 for r_1 (D – D) radial coordinate, and spherical oscillators with parameters 0, 0, and 0.016 for the r_2 (H – D_2 scattering coordinate). The dimension of the final vibrational Hamiltonians were set to 5000. Calculations included all levels up to 15000 cm^{-1} for $J \leq 25$. 1500 vibrational basis functions calculated using DVR3DRJZ were passed to ROTLEV3 for the rotational step of the calculation. Following Polyansky & Tennyson (1999), nuclear masses $m_{\text{H}} = 1.007276\text{ Da}$ and $m_{\text{D}} = 2.013553\text{ Da}$ were used for rotational motion and effective masses intermediate between nuclear and atomic masses $m_{\text{H}} = 1.007537\text{ Da}$ and $m_{\text{D}} = 2.013814\text{ Da}$ were used for the vibrational motion. This formulation has been shown to allow for non-adiabatic effects in the calculation. The resulting MiZo line list is complete up to a temperature of 2000 K.

3.4 D_3^+ nuclear motion calculations

DVR3D calculations for D_3^+ were performed using the same size grids and Hamiltonians as those specified for D_2H^+ above (31, 31, and 50 grid points for two radial and an angular scattering coordinates, correspondingly, and the final Hamiltonian dimensions equal to 5000). The calculations used Morse-like oscillators with parameters 2.6, 0.1, and 0.006 for the r_1 coordinate, and spherical oscillators with parameters 0, 0, and 0.016 for the r_2 coordinate. Nuclear masses equal to $m_{\text{D}} = 2.013553\text{ Da}$ were used for all calculations.

On the basis of nuclear motion calculation results and the DMS by Petrigani et al. (2014) a linelist in the frequency region up to 15000 cm^{-1} for a temperature of 800 K and using the corresponding partition function value 118.7 together with a list of corresponding energy levels for D_3^+ was computed. This linelist contains transitions between energy states with J values 0–15 and energies 0–15 500 cm^{-1} . The new MiZo D_3^+ line list is complete up to a temperature of 800 K.

Statistics for all of the line lists presented here are given in Table 7.

3.5 States files

New states files are provided for each of the four species considered here and are formatted using the standard outlined by Tennyson et al. (2013). H_3^+ and D_3^+ are identified using the same set of quantum numbers and hence their states files contain the same columns. Excerpts from the H_3^+ and D_3^+ states files are provided in Table 8. Similarly, the states files for H_2D^+ and D_2H^+ contain the same set of quantum number columns and an excerpts for them are shown in Table 9.

All entries in the new states files are marked with a source tag, indicating the method that was used to determine the final term energy for that level. Several values for the source tag can occur in ExoMol line lists (Bowesman et al. 2021) but only three are in use here: “Ma” for MARVELised energies, “EH” for energies from effective Hamiltonian calculations and “Ca” for energies calculated using DVR3D. For all levels marked “Ca” in all four states files an uncertainty estimate was calculated using Eq. (2).

All new and updated states files are ordered on increasing J , Γ_{rve} and energy. The existing H_2D^+ states file was already formatted this way, while H_3^+ was not and has been changed. Hence for H_3^+ the state counting number assigned to each level has been reassigned and the references to these values in the corresponding trans file have accordingly been updated. Excerpts from the trans files for the new D_2H^+ and D_3^+ line lists can be seen in Table 10.

In general all molecular states should be characterised by three rigorous quantum numbers: J , parity and the overall symmetry, which also determines the nuclear spin state (ortho/para/meta). All calculations have J and parity rigorously determined; due to the full treatment by DVR3D of the C_{2v} symmetry, the symmetry and nuclear spin statistics are also correctly determined for H_2D^+ and D_2H^+ . This is not the case for H_3^+ and D_3^+ however, as the program does not include a full treatment for a D_{3h} Hamiltonian. The symmetry was initially output for all molecular species considered here under C_{2v} symmetry, but was subsequently mapped to the appropriate D_{3h} representation for H_3^+ and D_3^+ for states with

Table 7. Statistics for the new line lists, detailing: the maximum J value for each; the maximum temperature up to which the line list is complete; the maximum lower state energy involved in a transition; the maximum upper state energy involved in a transition; the total number of transitions and the total number of transitions between MARVELised states.

Species	J_{\max}	T_{\max} (K)	E_{low} (cm^{-1})	E_{high} (cm^{-1})	No. Trans	No. MARVELised Trans
H_3^+	37	5000	25189.70934	42000.74357	127542657	17147
H_2D^+	20	1750	6988.91426	18496.21669	22164810	895
D_2H^+	25	2000	8253.939824	34838.528613	2290235000	905
D_3^+	15	800	2639.965597	17234.642274	36078183	0

Table 8. Excerpts from the H_3^+ and D_3^+ states files, using the format defined by [Tennyson et al. \(2013\)](#). Note that the zero-energy level of H_3^+ with A_1' symmetry does not exist and hence has “nan” entries for its lifetime and isomer. Any row for which the ν_1 , ν_2 , L_2 , G , U or K assignment is not known will likewise have “nan” entries in these columns.

i	\tilde{E}	g_{tot}	J	unc	τ	e/f	Γ_{rve}	No.	Isomer	ν_1	ν_2	L_2	G	U	K	Source Tag
H_3^+																
1	0.000000	0	0	0.000000	nan	e	A_1'	1	nan	0	0	0	0	m	0	Ma
2	2521.410484	2	0	0.000133	8.4474e-03	e	E'	1	p	0	1	1	1	m	0	Ma
3	4998.052947	2	0	0.010004	2.4871e-03	e	E'	2	p	0	2	2	2	m	0	Ma
4	5554.061000	2	0	0.010000	7.3144e-03	e	E'	3	p	1	1	1	1	m	0	Ca
5	7005.974780	2	0	0.010000	3.1660e-03	e	E'	4	p	0	3	1	1	m	0	Ca
6	7870.229810	2	0	0.010000	2.5047e-03	e	E'	5	p	1	2	2	2	m	0	Ca
7	8488.013160	2	0	0.010000	6.6336e-03	e	E'	6	p	2	1	1	1	m	0	Ca
8	9113.041390	2	0	0.010000	2.0836e-03	e	E'	7	p	0	4	2	2	m	0	Ca
9	9653.699850	2	0	0.010000	1.1122e-03	e	E'	8	p	1	3	1	1	m	0	Ca
10	9997.183130	2	0	0.010000	1.0631e-03	e	E'	9	p	0	4	4	4	m	0	Ca
D_3^+																
1	0.0000000	10	0	0.0000000	inf	+	A_1'	1	o	0	0	0	0	m	0	EH
2	2301.1985530	10	0	0.1000000	9.6693e+00	+	A_1'	2	o	1	0	0	0	m	0	Ca
3	3530.6654530	10	0	0.1000000	2.4171e-02	+	A_1'	3	o	0	2	0	0	m	0	Ca
4	4554.7949320	10	0	0.1000000	3.2217e+00	+	A_1'	4	o	2	0	0	0	m	0	Ca
5	5400.9592930	10	0	0.1000000	6.7375e-03	+	A_1'	5	o	0	3	3	3	m	0	Ca
6	5711.9821150	10	0	0.1000000	1.4546e-02	+	A_1'	6	o	1	2	0	0	m	0	Ca
7	6761.1836300	10	0	0.1000000	1.3900e+00	+	A_1'	7	o	3	0	0	0	m	0	Ca
8	6774.1319250	10	0	0.1000000	8.2880e-03	+	A_1'	8	o	0	4	0	0	m	0	Ca
9	7453.9598120	10	0	0.1000000	7.3275e-03	+	A_1'	9	o	1	3	3	3	m	0	Ca
10	8375.5588740	10	0	0.1000000	6.3728e-03	+	A_1'	10	o	0	5	3	3	m	0	Ca

i : State counting number;

\tilde{E} : Term value (in cm^{-1});

g_{tot} : Total state degeneracy;

J : Total angular momentum quantum number;

unc: Estimated uncertainty of energy level (in cm^{-1});

τ : Radiative lifetime (in seconds);

e/f: Rotationless parity;

Γ_{rve} : D_{3h} symmetry group;

No.: Symmetry group block counting number;

Isomer: Nuclear spin isomer;

ν_1 : Symmetric stretching quantum number;

ν_2 : Bending quantum number;

L_2 : Vibrational angular momentum quantum number;

G : Absolute value of $k - l_2$;

U : U -notation of [Watson \(1994\)](#);

K : Rotational angular momentum quantum number;

Source Tag: The method used to generate the term value; “Ma” for MARVELised energies, “EH” for energies from effective Hamiltonian calculations and “Ca” for energies calculated using DVR3D.

quantum number assignments. Due to the nuclear spin statistical weight of the A_1' , A_1'' symmetries in H_3^+ being 0, it was possible to map all of the C_{2v} symmetries to the appropriate D_{3h} representation ([Mizus et al. 2017](#)). For D_3^+ , where D_{3h} symmetry and quantum number assignment was not carried out, the entries retain the C_{2v} symmetries output by DVR3D. These C_{2v} symmetries are given as lower-case in the states file, to avoid confusion between the A_1 and A_2 irreducible representations under C_{2v} symmetry (formatted

as “a1” and “a2”) and the A_1' , A_1'' , A_2' and A_2'' irreducible representations under D_{3h} symmetry.

3.6 Partition Functions

Calculating the partition functions of the new line lists requires the determination of the total degeneracy of each state

Table 9. Excerpts from the H₂D⁺ and D₂H⁺ states files, using the format defined by [Tennyson et al. \(2013\)](#). Any row for which the ν_1 , ν_2 , ν_3 , K_a or K_c assignment is not known will have “nan” entries in these columns.

i	\bar{E}	g_{tot}	J	unc	τ	+/-	Γ_{rve}	No.	Isomer	ν_1	ν_2	ν_3	K_a	K_c	Source Tag
H ₂ D ⁺															
1	0.0000000	3	0	0.0000000	inf	+	A1	1	p	0	0	0	0	0	Ma
2	2205.8771127	3	0	0.0050000	5.7143e-02	+	A1	2	p	0	1	0	0	0	Ma
3	2992.5022357	3	0	0.0000050	1.8706e-02	+	A1	3	p	1	0	0	0	0	Ma
4	4287.4732000	3	0	0.2000000	1.8812e-02	+	A1	4	p	0	2	0	0	0	Ca
5	4602.6196400	3	0	0.2000000	3.1868e-03	+	A1	5	p	0	0	2	0	0	Ca
6	5039.7666100	3	0	0.2000000	1.9520e-02	+	A1	6	p	1	1	0	0	0	Ca
7	5877.2574100	3	0	0.2000000	1.0870e-02	+	A1	7	p	2	0	0	0	0	Ca
8	6287.6671127	3	0	0.0020000	6.4627e-03	+	A1	8	p	0	3	0	0	0	Ma
9	6645.7008700	3	0	0.3000000	2.5443e-03	+	A1	9	p	0	1	2	0	0	Ca
10	6991.5781127	3	0	0.0020000	9.4938e-03	+	A1	10	p	1	2	0	0	0	Ma
D ₂ H ⁺															
1	0.0000000	12	0	0.0000000	inf	+	A1	1	o	0	0	0	0	0	Ma
2	1968.1622648	12	0	0.0050000	1.9317e-02	+	A1	2	o	0	1	0	0	0	Ma
3	2736.9754969	12	0	0.0000040	1.1633e-02	+	A1	3	o	1	0	0	0	0	Ma
4	3821.2081670	12	0	0.1000000	1.2227e-02	+	A1	4	o	nan	nan	nan	nan	nan	Ca
5	4042.7721648	12	0	0.0009000	1.2305e-02	+	A1	5	o	0	0	2	0	0	Ma
6	4648.7587400	12	0	0.2000000	6.4298e-03	+	A1	6	o	nan	nan	nan	nan	nan	Ca
7	5385.3522270	12	0	0.2000000	6.0840e-03	+	A1	7	o	nan	nan	nan	nan	nan	Ca
8	5579.1928220	12	0	0.2000000	8.0766e-03	+	A1	8	o	nan	nan	nan	nan	nan	Ca
9	6008.5163100	12	0	0.3000000	4.8418e-03	+	A1	9	o	nan	nan	nan	nan	nan	Ca
10	6432.5596700	12	0	0.3000000	6.6492e-03	+	A1	10	o	nan	nan	nan	nan	nan	Ca

i : State counting number;

\bar{E} : Term value (in cm⁻¹);

g_{tot} : Total state degeneracy;

J : Total angular momentum quantum number;

unc: Estimated uncertainty of energy level (in cm⁻¹);

τ : Radiative lifetime (in seconds);

+/-: Total parity;

Γ_{rve} : C_{2v} symmetry group;

No.: Symmetry group block counting number;

Isomer: Nuclear spin isomer;

ν_1 : Symmetric stretching quantum number;

ν_2 : Bending quantum number;

ν_3 : Asymmetrical stretching quantum number;

K_a : Rotational angular momentum quantum number;

K_c : Rotational angular momentum quantum number;

Source Tag: The method used to generate the term value; “Ma” for MARVELised energies, “EH” for energies from effective Hamiltonian calculations and “Ca” for energies calculated using DVR3D.

considered, as show in [Eq. \(3\)](#):

$$z = \sum_i g_{\text{tot},i} \exp\left(-\frac{E_i}{k_B T}\right), \quad (3)$$

where g_{tot} is the total degeneracy of the i th level, E_i its energy, k_B is the Boltzmann constant and T is the temperature. The total degeneracy of a level depends directly on the nuclear spin statistical weight, g_{ns} :

$$g_{\text{tot}} = g_{\text{ns}}(2J + 1). \quad (4)$$

The nuclear spin statistical weights represent the number of nuclear spin functions that yield each symmetry. We follow the ExoMol and HITRAN convention of including the full nuclear spin degeneracy in our partition functions. In the case of H₃⁺, where each atom consists of one proton with $I = \frac{1}{2}$, Fermi statistics apply which results in no allowed configurations corresponding to the A₁['] or A₁^{''} representations. Accordingly, the g_{ns} values for these representations of H₃⁺ are 0, as shown in [Table 1](#). For D₃⁺ however, each Deuterium atom has $I = 1$ and is hence a boson, meaning additional

representations can occur that give rise to the “meta” nuclear spin isomer.

Our mappings of the C_{2v} representations output by DVR3D to the full D_{3h} symmetry are complete for all states presented in the H₃⁺ line list, but not for the states of D₃⁺. Hence, we must also consider the appropriate statistical weights to use when determining the degeneracy of the D₃⁺ states left with C_{2v} symmetries. As the D_{3h} representations A₁['], A₁^{''}, A₂['], A₂^{''}, E['], E^{''} correspond to A₁, A₂, B₂, B₁, A₁ ⊕ B₂, A₂ ⊕ B₁ respectively under C_{2v} symmetry, we can calculate population weighted average statistical weights for each C_{2v} representation. These are calculated knowing that approximately two thirds of all D₃⁺ levels will be E['] and E^{''}, due to the constraint that A₁['], A₁^{''}, A₂['] and A₂^{''} levels only occur when $G = 3n$, where n is an integer; see also [Berblinger et al. \(1992\)](#). Accordingly, for the A₁ and A₂ representations in C_{2v} symmetry, one third will be A₁['] or A₁^{''} under D_{3h} symmetry while the remaining two thirds will be E['] and E^{''}. The equivalent population ratio is true for B₁ and B₂ states and the corresponding A₂['] and A₂^{''} representations. These population ratios are then weighted using the weights from [Table 1](#),

Table 10. Excerpts from the trans files for the new line lists for D_2H^+ and D_3^+ .

D_2H^+			D_3^+		
f	i	A_{fi} (s^{-1})	f	i	A_{fi} (s^{-1})
1401	1	3.30142477E-03	226	16	5.65667085E-09
1402	2	2.19499998E-03	229	16	2.93922054E-02
3	1402	1.59575873E-01	216	226	1.30736782E-07
1403	2	1.80478736E-03	1023	226	4.95756630E-07
3	1403	4.59507405E-02	1025	226	5.90452177E-07
1404	2	9.63358275E-02	1028	226	6.58440901E-02
1404	3	3.99647847E-03	2	212	1.03419866E-01
1405	4	2.49561352E-03	1013	212	2.22162053E-02
5	1405	2.09336332E-03	229	216	3.39285830E-02
6	1405	3.28445005E-01	1043	216	4.03805710E-07

f : The upper state counting number from the corresponding states file.

i : The lower state counting number from the corresponding states file.

A_{fi} : The Einstein A coefficient.

Table 11. Adjusted nuclear spin statistical weights for the levels of D_3^+ for which C_{2v} symmetries are used.

Γ_{rve}	g_{ns}
A ₁ , A ₂	6
B ₁ , B ₂	3

yielding the g_{ns} values shown in Table 11. These adjusted weights were used to calculate the total degeneracies of the states of the D_3^+ line list for which C_{2v} symmetries are used and are included in the new states file.

Partition functions are given in Table 12 for a series of temperatures up to the value of T_{max} for each line list. Partition functions for D_3^+ had previously been calculated by Ramanlal & Tennyson (2004) and their values are in close agreement with those presented here. For H_2D^+ however, the partition functions differ from those given by Sochi & Tennyson (2010). This is due to the different nuclear spin statistical weights used in their earlier work that did not consider the spin of the Deuterium atom. The degeneracies given in the H_2D^+ line list have been updated to use the nuclear spin statistical weights quoted in Table 1 and are thus consistent with the partition function computed using Eq. (3) and the same convention.

4 SPECTRA

4.1 Rotational Spectra

Purely rotational transitions within the vibrational ground states are important for detections of H_3^+ and particularly its deuterated isotopologues in the interstellar medium. This is due to the low temperatures in such regions driving the majority of the level populations to low-energy states. Predicted transition frequencies for such transitions are given in Table 13 for H_3^+ and D_3^+ and in Table 14 for H_2D^+ and D_2H^+ , based on the term energies derived from the MARVEL networks presented here. While the purely rotational transitions of H_3^+ are “forbidden” due to the lack of a permanent electric dipole moment, it is believed that a small, temporary dipole moment can be induced due to the distortion of the molecule from equilibrium geometry under rotation about

Table 12. The partition functions for each new line list, calculated for a range of temperatures up to each line list’s maximum temperature, given in Table 7.

Temp. (K)	H_3^+	H_2D^+	D_2H^+	D_3^+
10	6.0000×10^{-4}	3.0181×10^0	1.2153×10^1	1.0235×10^1
50	2.0215×10^0	1.5141×10^1	3.7355×10^1	2.7175×10^1
100	7.3972×10^0	4.5354×10^1	9.7278×10^1	6.9095×10^1
200	2.0733×10^1	1.2604×10^2	2.6721×10^2	1.9085×10^2
300	3.7609×10^1	2.2937×10^2	4.8756×10^2	3.4904×10^2
400	5.7650×10^1	3.5231×10^2	7.5053×10^2	5.3858×10^2
500	8.0581×10^1	4.9357×10^2	1.0549×10^3	7.6022×10^2
600	1.0640×10^2	6.5391×10^2	1.4048×10^3	1.0188×10^3
700	1.3533×10^2	8.3572×10^2	1.8080×10^3	1.3215×10^3
800	1.6783×10^2	1.0426×10^3	2.2746×10^3	1.6761×10^3
900	2.0442×10^2	1.2787×10^3	2.8162×10^3	
1000	2.4578×10^2	1.5489×10^3	3.4456×10^3	
1250	3.7478×10^2	2.4087×10^3	5.4967×10^3	
1500	5.5089×10^2	3.6069×10^3	8.4351×10^3	
1750	7.8938×10^2	5.2510×10^3	1.2563×10^4	
2000	1.1086×10^3		1.8242×10^4	
3000	3.7032×10^3			
4000	1.0239×10^4			
5000	2.4177×10^4			

the C_2 molecular axis (Pan & Oka 1986; Miller & Tennyson 1988).

The D_3^+ states file contains 43 extremely long-lived states with radiative lifetimes greater than 10^{10} s and can be considered meta-stable. In the extreme case, two states are calculated to have radiative lifetimes greater than 10^{18} s, a duration greater than the current age of the universe. All of these meta-stable states are in the vibrational ground state and have $G = J$ or $G = J - 1$. The same is true for the meta-stable states of H_3^+ , though only one of their radiative lifetimes is in excess of 10^{10} s. In both species, this can cause molecules to become “trapped” in these states in collision free environments with consequences for both laboratory measurements (Kreckel et al. 2004) and for possible maser action.

4.2 Mid and Far Infrared Spectra

Fig. 1 shows example stick spectra for H_3^+ and its deuterated isotopologues in the far infrared region from 10 - 1000 cm^{-1} . These spectra were generated using the program EXOCROSS (Yurchenko et al. 2018) and were computed for a temperature of 200 K. The predicted transitions frequencies listed in Tables 13 and 14 that are expected to be of importance in the ISM fall within this range. Likewise, spectra were computed for the mid infrared region between 1000 - 5000 cm^{-1} for all species considered here and are shown in Fig. 2. These cover several wavelength ranges where H_3^+ has been observed in Jupiter’s aurorae, such as the K band region centred at 2.2 μm (Uno et al. 2014) and the L band centred on 3.5 μm (Baron et al. 1991). This also covers the wavelength regions observed using the Jupiter infrared Auroral Mapper (JIRAM) instrument onboard NASA’s Juno spacecraft (Dinelli et al. 2019; Migliorini et al. 2019) and those covered by the Near infrared Camera (NIRCam) long-wavelength channel onboard JWST.

Comparisons between computed spectra and real observations cannot be made for H_2D^+ , D_2H^+ and D_3^+ , as no measured transition intensities have been published. McKellar &

Watson (1998) presented infrared absorption spectra of the ν_2 fundamental band of H_3^+ and provided integrated intensities, which were well reproduced by the original line list (Mizus et al. 2017).

5 CONCLUSION

We have updated three MARVEL networks for H_3^+ , H_2D^+ and D_2H^+ to include all currently published spectroscopic data for these molecules. We have also performed variational nuclear motion calculations using the program DVR3D for D_2H^+ and D_3^+ to produce the new MiZo line lists. The empirical energy levels derived from the MARVEL networks have been used to update the calculated levels of their respective molecules. This allows for the subset of transitions involving these MARVELised energies to be determined to much higher accuracy, making the use of these line lists well suited for high-resolution spectroscopy. The D_3^+ calculations have been combined with a set of energies derived from effective Hamiltonian calculations computed using experimentally determined molecular constants. Given these effective Hamiltonian constants were derived from transitions in infrared bands, the new D_3^+ line list is best suited for infrared studies. Overall, the new D_3^+ line list is of lower resolution than the other three, due to the lack of MARVELised energy levels.

Hyperfine effects are known to be present in the spectra of H_3^+ and its deuterated isotopologues, due to the nuclear spin of the component protons and deuterons (Jensen et al. 1997). These hyperfine splittings have not yet been observed however in either an astrophysical setting or in the laboratory. Were experiments to be conducted to measure the hyperfine-resolved spectra of the species considered here, it would enable the construction of a hyperfine-resolved MARVEL network and subsequently line lists. Similarly, any further measurements of hyperfine-unresolved spectra could be added to the current MARVEL network to further constrain the resultant empirical energy levels and hence improve the accuracy of the line lists. If a sufficiently large number of spectra were observed for D_3^+ to form a well-connected spectroscopic network, it would enable us to further update the D_3^+ line list with MARVEL energies to a high-resolution standard.

The four line lists presented here, each consisting of a states file and transitions file, are made available via www.exomol.com.

ACKNOWLEDGEMENTS

We thank Tibor Furtenbacher and Attila Császár for supplying the MARVEL4 code and for helpful discussions during the course of this work. This work was supported by the European Research Council (ERC) under the European Union's Horizon 2020 research and innovation programme through Advance Grant number 883830 and the UK STFC under grant ST/R000476/1. BP acknowledges support from the US National Science Foundation (CHE-1665370), and the Robert A. Welch Foundation (D-1523). NFZ and OLP acknowledge support by State Project IAP RAS No. 0030-2021-0016. JS is grateful to NKFIH for support (PD142580).

Figure 1. Far infrared spectra for H_3^+ and its deuterated isotopologues, computed using the program EXOCROSS (Yurchenko et al. 2018) at 200 K between 10 - 1000 cm^{-1} (1 mm - 10 μm).

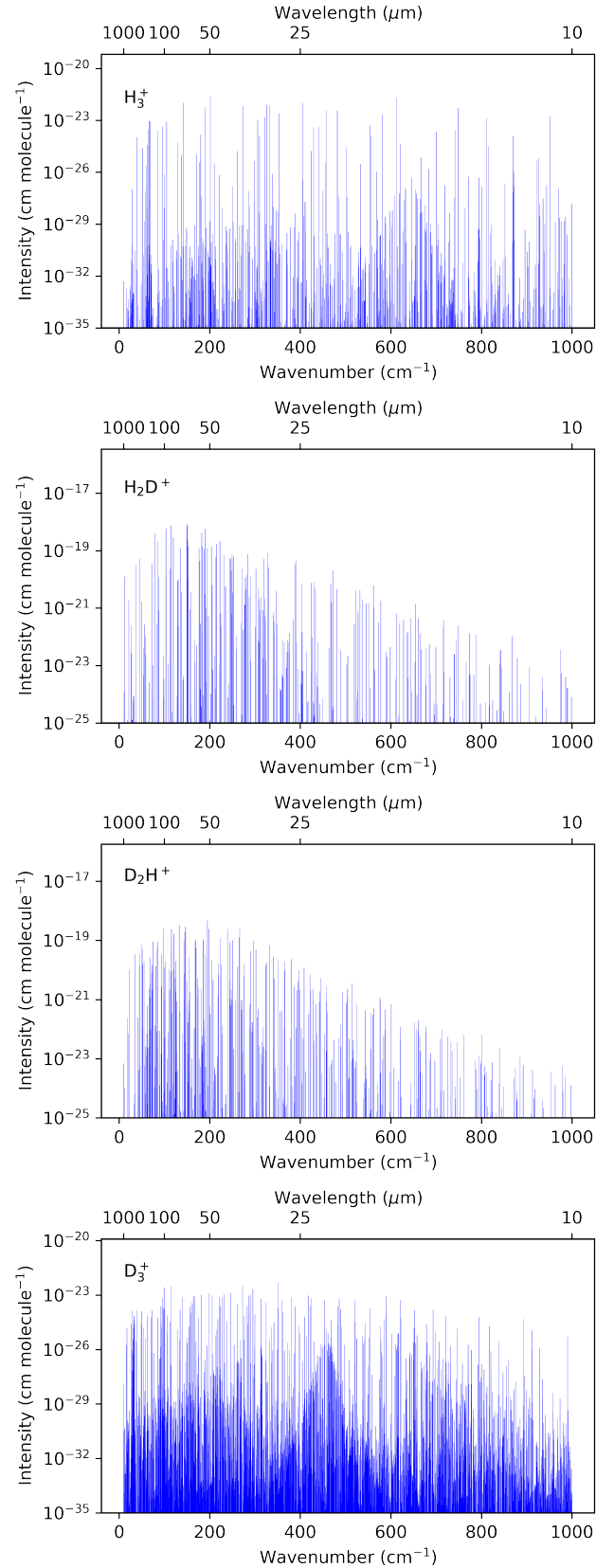


Table 13. Predicted pure-rotation transition wavenumbers and Einstein A coefficients for transitions involving low-energy lower levels for H_3^+ and D_3^+ . For all upper and lower levels included here, $\nu_1 = \nu_2 = L_2 = 0$. Values quoted in brackets for energies are the uncertainty in the last digit.

Wavenumber (cm^{-1})	A_{fi} (s^{-1})	Upper Level						Lower Level					
		J	G	U	K	Γ_{rve}	Term Energy (cm^{-1})	J	G	U	K	Γ_{rve}	Term Energy (cm^{-1})
H_3^+													
105.17639(37)	4.2570×10^{-7}	2	2	m	2	E'	169.29739(37)	1	1	m	1	E''	64.121000(0)
68.05481(37)	5.6141×10^{-7}	2	1	m	1	E''	237.352195(50)	2	2	m	2	E'	169.29739(37)
325.46535(40)	3.4982×10^{-5}	3	1	m	1	E''	494.76274(14)	2	2	m	2	E'	169.29739(37)
190.66548(40)	1.7422×10^{-5}	3	2	m	2	E'	428.01768(39)	2	1	m	1	E''	237.352195(50)
201.52843(29)	7.3590×10^{-5}	3	0	m	0	A'_2	516.88036(23)	3	3	m	3	A''_2	315.35192(18)
66.74506(42)	2.6423×10^{-6}	3	1	m	1	E''	494.76274(14)	3	2	m	2	E'	428.01768(39)
405.55623(42)	3.2067×10^{-4}	4	1	m	1	E''	833.57391(14)	3	2	m	2	E'	428.01768(39)
7.27431(27)	2.5602×10^{-9}	4	4	m	4	E'	502.03705(23)	3	1	m	1	E''	494.76274(14)
273.70656(44)	1.7953×10^{-4}	4	2	m	2	E'	768.46930(42)	3	1	m	1	E''	494.76274(14)
D_3^+													
53.3000(28)	1.3067×10^{-8}	2	2	m	2	E'	85.6210(20)	1	1	m	1	E''	32.3210(20)
33.7470(28)	1.6552×10^{-8}	2	1	m	1	E''	119.3680(20)	2	2	m	2	E'	85.6210(20)
163.7280(28)	1.0739×10^{-6}	3	1	m	1	E''	249.3490(20)	2	2	m	2	E'	85.6210(20)
96.5440(28)	5.5135×10^{-7}	3	2	m	2	E''	215.9120(20)	2	1	m	1	E''	119.3680(20)
29.2810(28)	3.1041×10^{-8}	3	-3	m	3	A''_1	159.8680(20)	2	0	m	0	A'_1	130.5870(20)
100.5990(28)	2.1970×10^{-6}	3	0	m	0	A'_2	260.4660(20)	3	3	m	3	A''_2	159.8670(20)
272.6900(28)	1.4422×10^{-5}	4	0	m	0	A'_1	432.5580(20)	3	-3	m	3	A''_1	159.8680(20)
33.4370(28)	8.0083×10^{-8}	3	1	m	1	E''	249.3490(20)	3	2	m	2	E'	215.9120(20)
205.6600(28)	1.0260×10^{-5}	4	1	m	1	E''	421.5720(20)	3	2	m	2	E'	215.9120(20)
5.6660(28)	3.0205×10^{-10}	4	4	m	4	E'	255.0150(20)	3	1	m	1	E''	249.3490(20)
139.0820(28)	5.7366×10^{-6}	4	2	m	2	E'	388.4310(20)	3	1	m	1	E''	249.3490(20)

DATA AVAILABILITY

The updated MARVEL input files and resulting output energy levels are given as supporting material. All other data are available via the www.exomol.com website.

REFERENCES

- Al-Derzi A. R., et al., 2021, *J. Quant. Spectrosc. Radiat. Transf.*, 266, 107563
- Alijah A., Wolniewicz L., Hinze J., 1995, *Mol. Phys.*, 85, 1125
- Amano T., 1985, *J. Opt. Soc. Am. B*, 2, 790 – 793
- Amano T., 2006, *Phil. Trans. Royal Soc. London A*, 364, 2943
- Amano T., Hirao T., 2005, *J. Mol. Spectrosc.*, 233, 7
- Amano T., Watson J. K. G., 1984, *J. Chem. Phys.*, 81, 2869
- Amano T., Chan M. C., Civis S., McKellar A. R. W., Majewski W. A., Sadovskii D., Watson J. K. G., 1994, *Can. J. Phys.*, 72, 1007
- Asvany O., Hugo E., Schlemmer S., Muller F., Kuhnemann F., Schiller S., Tennyson J., 2007, *J. Chem. Phys.*, 127, 154317
- Asvany O., Ricken O., Müller H.-S.-P., Wiedner M.-C., Giesen T.-F., Schlemmer S., 2008, *Phys. Rev. Lett.*, 100, 233004
- Ballester G. E., Miller S., Tennyson J., Trafton L. M., Geballe T. R., 1994, *Icarus*, 107, 189
- Baron R., Joseph R. D., Owen T., Tennyson J., Miller S., Ballester G. E., 1991, *Nature*, 353, 539
- Bawendi M. G., Rehfuss B. D., Oka T., 1990, *J. Chem. Phys.*, 93, 6200
- Berblinger M., Schlier C., Tennyson J., Miller S., 1992, *J. Chem. Phys.*, 96, 6842
- Berg M., Wolf A., Petrigiani A., 2012, *Phil. Trans. Royal Soc. London A*, 370, 5028
- Bergeron P., Ruiz M. T., Leggett S. K., 1997, *Astrophys. J. Suppl.*, 108, 339
- Bogey M., Demuyne C., Denis M., Destombes J. L., Lemoine B., 1984, *Astron. Astrophys.*, 137, L15
- Bowesman C. A., Shuai M., Yurchenko S. N., Tennyson J., 2021, *Mon. Not. R. Astron. Soc.*, 508, 3181
- Bowesman C. A., Akbari H., Hopkins S., Yurchenko S. N., Tennyson J., 2022, *J. Quant. Spectrosc. Radiat. Transf.*, 289, 108295
- Caselli P., van der Tak F. F. S., Ceccarelli C., Bacmann A., 2003, *Astron. Astrophys.*, 403, L37
- Chadney J. M., Galand M., Koskinen T. T., Miller S., Sanz-Forcada J., Unruh Y. C., Yelle R. V., 2016, *Astron. Astrophys.*, 587, A87
- Chen W., Poirier B., 2006a, *J. Comput. Phys.*, 219, 185
- Chen W., Poirier B., 2006b, *J. Comput. Phys.*, 219, 198
- Chen W., Poirier B., 2010a, *J. Theoret. Comput. Chem.*, 9, 825
- Chen W., Poirier B., 2010b, *J. Parallel Distrib. Comput.*, 70, 779
- Crabtree K. N., Hodges J. N., Siller B. M., Perry A. J., Kelly J. E., Jenkins P. A., McCall B. J., 2012, *Chem. Phys. Lett.*, 551, 1
- Császár A. G., Furtenbacher T., 2011, *J. Mol. Spectrosc.*, 266, 99
- Dinelli B. M., Neale L., Polyansky O. L., Tennyson J., 1997, *J. Mol. Spectrosc.*, 181, 142
- Dinelli B. M., Adriani A., Mura A., Altieri F., Migliorini A., Moriconi M. L., 2019, *Phil. Trans. Royal Soc. London A*, 377, 20180406
- Drossart P., et al., 1989, *Nature*, 340, 539
- Fábrí C., Mátyus E., Császár A. G., 2011, *J. Chem. Phys.*, 134, 074105
- Farnik M., Davis S., Kostin M. A., Polyansky O. L., Tennyson J., Nesbitt D. J., 2002, *J. Chem. Phys.*, 116, 6146
- Foster S. C., McKellar A. R. W., Peterkin I. R., Watson J. K. G., Pan F. S., Crofton M. W., Altman R. S., Oka T., 1986a, *J. Chem. Phys.*, 84, 91
- Foster S. C., McKellar A. R. W., Watson J. K. G., 1986b, *J. Chem. Phys.*, 85, 664
- Furtenbacher T., Császár A. G., 2012, *J. Quant. Spectrosc. Radiat. Transf.*, 113, 929
- Furtenbacher T., Császár A. G., Tennyson J., 2007, *J. Mol. Spectrosc.*, 245, 115
- Furtenbacher T., Szidarovszky T., Mátyus Edit Fábrí C., Császár A. G., 2013a, *J. Chem. Theory Comput.*, 9, 5471

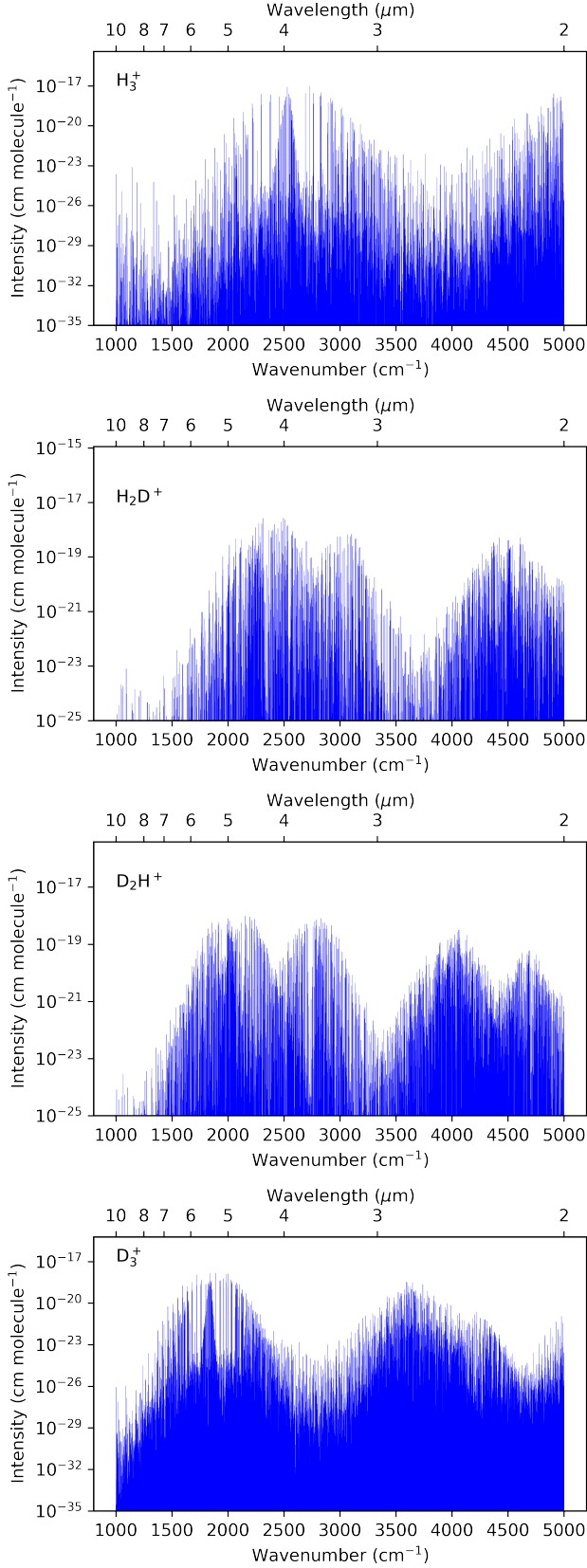
Table 14. Predicted pure-rotation transition wavenumbers and Einstein A coefficients for transitions involving low-energy lower levels for H_2D^+ and D_2H^+ . For all upper and lower levels included here, $\nu_1 = \nu_2 = \nu_3 = 0$. Values quoted in brackets for the transition frequencies are the uncertainty in the last digit.

Wavenumber (cm^{-1})	A_{fi} (s^{-1})	J	K_a	K_c	Upper Level		Lower Level				
					Γ_{rve}	Term Energy (cm^{-1})	J	K_a	K_c	Γ_{rve}	Term Energy (cm^{-1})
H_2D^+											
45.7011127(4)	4.0400×10^{-3}	1	0	1	A ₂	45.7011127(4)	0	0	0	A ₁	0.0000000(0)
85.951350(33)	3.0300×10^{-2}	2	0	2	A ₁	131.652463(33)	1	0	1	A ₂	45.7011127(4)
178.1566(36)	1.6600×10^{-2}	2	2	0	A ₁	223.8577(36)	1	0	1	A ₂	45.7011127(4)
12.422639(14)	1.2200×10^{-4}	1	1	0	B ₂	72.452486(10)	1	1	1	B ₁	60.029846(10)
78.829277(23)	1.8800×10^{-2}	2	1	2	B ₂	138.859124(21)	1	1	1	B ₁	60.029846(10)
103.482549(23)	4.2400×10^{-2}	2	1	1	B ₁	175.935034(21)	1	1	0	B ₂	72.452486(10)
87.0021(36)	3.2700×10^{-3}	2	2	1	A ₂	218.6545(36)	2	0	2	A ₁	131.652463(33)
119.7622(20)	8.5300×10^{-2}	3	0	3	A ₂	251.4146(20)	2	0	2	A ₁	131.652463(33)
244.6884(70)	4.7600×10^{-2}	3	2	1	A ₂	376.3409(70)	2	0	2	A ₁	131.652463(33)
37.075911(30)	1.0700×10^{-3}	2	1	1	B ₁	175.935034(21)	2	1	2	B ₂	138.859124(21)
115.201469(33)	7.3200×10^{-2}	3	1	3	B ₁	254.060593(26)	2	1	2	B ₂	138.859124(21)
319.4843(70)	2.3600×10^{-2}	3	3	1	B ₁	458.3434(70)	2	1	2	B ₂	138.859124(21)
150.2252(20)	1.5900×10^{-1}	3	1	2	B ₂	326.1602(20)	2	1	1	B ₁	175.935034(21)
283.8945(70)	3.7500×10^{-2}	3	3	0	B ₂	459.8296(70)	2	1	1	B ₁	175.935034(21)
5.2032(50)	1.1300×10^{-5}	2	2	0	A ₁	223.8577(36)	2	2	1	A ₂	218.6545(36)
136.1238(79)	7.7800×10^{-2}	3	2	2	A ₁	354.7783(70)	2	2	1	A ₂	218.6545(36)
27.5569(41)	9.5600×10^{-6}	3	0	3	A ₂	251.4146(20)	2	2	0	A ₁	223.8577(36)
152.4832(79)	1.1200×10^{-1}	3	2	1	A ₂	376.3409(70)	2	2	0	A ₁	223.8577(36)
103.3637(73)	8.2700×10^{-3}	3	2	2	A ₁	354.7783(70)	3	0	3	A ₂	251.4146(20)
151.38(10)	1.8100×10^{-1}	4	0	4	A ₁	402.80(10)	3	0	3	A ₂	251.4146(20)
329.972(10)	6.7000×10^{-2}	4	2	2	A ₁	581.386(10)	3	0	3	A ₂	251.4146(20)
527.62(10)	4.6500×10^{-3}	4	4	0	A ₁	779.04(10)	3	0	3	A ₂	251.4146(20)
72.0997(20)	4.1900×10^{-3}	3	1	2	B ₂	326.1602(20)	3	1	3	B ₁	254.060593(26)
149.6189(53)	1.7400×10^{-1}	4	1	4	B ₂	403.6795(53)	3	1	3	B ₁	254.060593(26)
205.7690(70)	3.1700×10^{-3}	3	3	0	B ₂	459.8296(70)	3	1	3	B ₁	254.060593(26)
391.51(10)	5.2800×10^{-2}	4	3	2	B ₂	645.57(10)	3	1	3	B ₁	254.060593(26)
D_2H^+											
49.2542648(2)	3.3014×10^{-3}	1	1	1	A ₂	49.2542648(2)	0	0	0	A ₁	0.0000000(0)
23.071309(14)	5.0885×10^{-4}	1	1	0	B ₂	57.989629(10)	1	0	1	B ₁	34.918320(10)
75.341734(30)	1.0592×10^{-2}	2	1	2	B ₂	110.260054(28)	1	0	1	B ₁	34.918320(10)
52.4637522(33)	2.0691×10^{-3}	2	0	2	A ₁	101.7180170(33)	1	1	1	A ₂	49.2542648(2)
132.809827(10)	4.4605×10^{-2}	2	2	0	A ₁	182.064091(10)	1	1	1	A ₂	49.2542648(2)
121.174679(68)	4.4481×10^{-2}	2	2	1	B ₁	179.164308(67)	1	1	0	B ₂	57.989629(10)
34.6460731(47)	1.2985×10^{-3}	2	1	1	A ₂	136.3640901(34)	2	0	2	A ₁	101.7180170(33)
98.3110072(57)	2.4763×10^{-2}	3	1	3	A ₂	200.0290242(47)	2	0	2	A ₁	101.7180170(33)
68.904254(73)	4.5854×10^{-3}	2	2	1	B ₁	179.164308(67)	2	1	2	B ₂	110.260054(28)
85.840024(73)	1.4620×10^{-2}	3	0	3	B ₁	196.100078(67)	2	1	2	B ₂	110.260054(28)
185.781201(73)	5.4468×10^{-2}	3	2	1	B ₁	296.041254(67)	2	1	2	B ₂	110.260054(28)
45.700001(11)	2.2792×10^{-3}	2	2	0	A ₁	182.064091(10)	2	1	1	A ₂	136.3640901(34)
146.951256(94)	6.2260×10^{-2}	3	2	2	A ₁	283.315346(94)	2	1	1	A ₂	136.3640901(34)
72.137151(95)	1.7139×10^{-3}	3	1	2	B ₂	251.301459(67)	2	2	1	B ₁	179.164308(67)
17.964933(11)	5.6565×10^{-6}	3	1	3	A ₂	200.0290242(47)	2	2	0	A ₁	182.064091(10)
55.201381(95)	3.5511×10^{-3}	3	1	2	B ₂	251.301459(67)	3	0	3	B ₁	196.100078(67)
121.1511(50)	5.0954×10^{-2}	4	1	4	B ₂	317.2512(50)	3	0	3	B ₁	196.100078(67)
83.286322(94)	8.5394×10^{-3}	3	2	2	A ₁	283.315346(94)	3	1	3	A ₂	200.0290242(47)
115.707967(94)	4.3474×10^{-2}	4	0	4	A ₁	315.736992(94)	3	1	3	A ₂	200.0290242(47)
44.739796(95)	2.9105×10^{-3}	3	2	1	B ₁	296.041254(67)	3	1	2	B ₂	251.301459(67)
168.1638(50)	8.7250×10^{-2}	4	2	3	B ₁	419.4653(50)	3	1	2	B ₂	251.301459(67)
115.73401(13)	1.5816×10^{-2}	4	1	3	A ₂	399.049356(97)	3	2	2	A ₁	283.315346(94)
240.0720(50)	2.4471×10^{-1}	4	3	1	A ₂	523.3873(50)	3	2	2	A ₁	283.315346(94)
21.2099(50)	6.8544×10^{-6}	4	1	4	B ₂	317.2512(50)	3	2	1	B ₁	296.041254(67)

Furtenbacher T., Szidarovszky T., Fábri C., Császár A. G., 2013b, *Phys. Chem. Chem. Phys.*, 15, 10181
 Geballe T. R., Oka T., 1996, *Nature*, 384, 334
 Geballe T. R., Jagod M. F., Oka T., 1993, *Astrophys. J.*, 408, L109
 Gibbs A., Fitzgerald M. P., 2022, *Astron. J.*, 164
 Gottfried J. L., McCall B. J., Oka T., 2003, *J. Chem. Phys.*, 118, 10890
 Guan Y.-C., Chang Y.-H., Liao Y.-C., Peng J.-L., Wang L.-B., Shy

J.-T., 2018, *J. Chem. Phys.*, 148, 124310
 Harju J., et al., 2017, *Astrophys. J.*, 840, 63
 Hewitt A. J., Doss N., Zobov N. F., Polyansky O. L., Tennyson J., 2005, *Mon. Not. R. Astron. Soc.*, 356, 1123
 Hirao T., Amano T., 2003, *Astrophys. J.*, 597, L85
 Hlavinka P., Korolov I., Plasil R., Varju J., Kotrik T., Glosik J., 2006a, *Czech. J. Phys.*, 56, B749
 Hlavinka P., Plasil R., Bano G., Korolov I., Ramanlal J., Tennyson

Figure 2. Mid infrared spectra for H_3^+ and its deuterated isotopologues, computed using the program EXOCROSS (Yurchenko et al. 2018) at 200 K between 1000 - 5000 cm^{-1} (10 - 2 μm).



- J., Glosik J., Gerlich D., 2006b, *Intern. J. Mass Spectrometry*, 255-256, 170
- Hodges J. N., Perry A. J., Jenkins II P. A., Siller B. M., McCall B. J., 2013, *J. Chem. Phys.*, 139, 164201
- Hougen J. T., 1962, *J. Chem. Phys.*, 37, 1433
- Indriolo N., McCall B. J., 2012, *Astrophys. J.*, 745, 91
- Jaquet R., 2022, *J. Mol. Spectrosc.*, 384, 111585
- Jensen P., Páidarová I., Špirko V., Sauer S. P. A., 1997, *Mol. Phys.*, 91, 319
- Jusko P., Konietzko C., Schlemmer S., Asvany O., 2016, *J. Mol. Spectrosc.*, 319, 55
- Jusko P., Toepfer M., Mueller H. S. P., Ghosh P. N., Schlemmer S., Asvany O., 2017, *J. Mol. Spectrosc.*, 332, 33
- Kao L., Oka T., Miller S., Tennyson J., 1991, *Astrophys. J. Suppl.*, 77, 317
- Khodachenko M. L., Shaikhislamov I. F., Lammer H., Prokopov P. A., 2015, *Astrophys. J.*, 813, 50
- Koskinen T. T., Aylward A. D., Miller S., 2007, *Nature*, 450, 845
- Kreckel H., Schwalm D., Tennyson J., Wolf A., Zaffman D., 2004, *New J. Phys*, 6, 151
- Kreckel H., Bing D., Reinhardt S., Petrigiani A., Berg M. H., Wolf A., 2008, *J. Chem. Phys.*, 129, 164312
- Lam H. A., Miller S., Joseph R. D., Geballe T. R., Trafton L. M., Tennyson J., Ballester G. E., 1997, *Astrophys. J.*, 474, L73
- Lee S. S., Ventruolo B. F., Cassidy D. T., Oka T., Miller S., Tennyson J., 1991, *J. Mol. Spectrosc.*, 145, 222
- Lenz L. F., Reiners A., Seifahrt A., Kaeuff H. U., 2016, *Astron. Astrophys.*, 589, A99
- Lindsay C. M., McCall B. J., 2001, *J. Mol. Spectrosc.*, 210, 60
- Lindsay C. M., Rade Jr R. M., Oka T., 2001, *J. Mol. Spectrosc.*, 210, 51
- Lubic K. G., Amano T., 1984, *Can. J. Phys.*, 62, 1886
- Majewski W., Marshall M. D., McKellar A., Johns J., Watson J., 1987, *J. Mol. Spectrosc.*, 122, 341
- Majewski W. A., Feldman P. A., Watson J. K. G., Miller S., Tennyson J., 1989, *Astrophys. J.*, 347, L51
- Majewski W. A., McKellar A. R. W., Sadovskii D., Watson J. K. G., 1994, *Can. J. Phys.*, 72, 1016
- Markus C. R., McCall B. J., 2019, *J. Chem. Phys.*, 150, 214303
- Markus C. R., McCall B. J., Schrader A. W., Esposito A. M., Kocheril P. A., 2018, in *73rd International Symposium on Molecular Spectroscopy*. p. MG09, doi:10.15278/isms.2018.MG09
- Markus C. R., Kocheril P. A., McCall B. J., 2019, *J. Mol. Spectrosc.*, 355, 8
- Mátyus E., Czakó G., Császár A. G., 2009, *J. Chem. Phys.*, 130, 134112
- Mátyus E., Fábri C., Szidarovszky T., Czakó G., Allen W. D., Császár A. G., 2010, *J. Chem. Phys.*, 133, 034113
- McCall B. J., Oka T., 2000, *J. Chem. Phys.*, 113, 3104
- McKellar A., Watson J., 1998, *J. Mol. Spectrosc.*, 191, 215
- Melin H., Stallard T., Miller S., Lystrup M. B., Trafton L. M., Booth T. C., Rivers C., 2011, *Mon. Not. R. Astron. Soc.*, 410, 641
- Melin H., Fletcher L. N., Stallard T. S., Johnson R. E., O'Donoghue J., Moore L., Donnelly P. T., 2018, *Mon. Not. R. Astron. Soc.*, 474, 3714
- Melin H., et al., 2019, *Phil. Trans. Royal Soc. London A*, 377, 20180408
- Merkt F., Hoeveler K., Deiglmayr J., 2022, *J. Phys. Chem. Lett.*
- Migliorini A., et al., 2019, *Icarus*, 329, 132
- Mikosch J., Kreckel H., Wester R., Plašil R., Glosík J., Gerlich D., Schwalm D., Wolf A., 2004, *J. Chem. Phys.*, 121, 11030
- Miller S., Tennyson J., 1988, *Astrophys. J.*, 335, 486
- Miller S., Achilleos N., Ballester G. E., Lam H. A., Tennyson J., Geballe T. R., Trafton L. M., 1997, *Icarus*, 130, 57
- Miller S., Stallard T., Melin H., Tennyson J., 2010, *Faraday Discuss.*, 147, 283

- Miller S., Geballe T. R., Stallard T., Tennyson J., 2020, *Rev. Mod. Phys.*, 92, 035003
- Mizus I. I., Alijah A., Zobov N. F., Kyuberis A. A., Yurchenko S. N., Tennyson J., Polyansky O. L., 2017, *Mon. Not. R. Astron. Soc.*, 468, 1717
- Moore L., et al., 2017, *Geophys. Res. Lett.*, 44, 4513
- Morong C. P., Gottfried J. L., Oka T., 2009, *J. Mol. Spectrosc.*, 255, 13
- Nakanaga T., Ito F., Sugawara K., Takeo H., Matsumura C., 1990, *Chemical Physics Letters*, 169, 269
- Neale L., Tennyson J., 1995, *Astrophys. J.*, 454, L169
- Neale L., Miller S., Tennyson J., 1996, *Astrophys. J.*, 464, 516
- Oka T., 1980, *Phys. Rev. Lett.*, 45, 531
- Oka T., 1981, *Phil. Trans. Royal Soc. London A*, 303, 543
- Oka T., 2006, *Proc. Nat. Acad. Sci.*, 103, 12235
- Oka T., Epp E., 2004, *Astrophys. J.*, 613, 349
- Owens A., Dooley S., McLaughlin L., Tan B., Zhang G., Yurchenko S. N., Tennyson J., 2022, *Mon. Not. R. Astron. Soc.*, 511, 5448
- Pan F. S., Oka T., 1986, *Astrophys. J.*, 305, 518
- Pavanello M., et al., 2012a, *Phys. Rev. Lett.*, 108, 023002
- Pavanello M., et al., 2012b, *J. Chem. Phys.*, 136, 184303
- Perry A. J., Hodges J. N., Markus C. R., Kocheril G. S., McCall B. J., 2015, *J. Mol. Spectrosc.*, 317, 71
- Perry A. J., McCall B. J., Kocheril G. S., Hodges J. N., Markus C. R., 2016, in 71st International Symposium on Molecular Spectroscopy. p. MH03, doi:10.15278/isms.2016.MH03
- Petrignani A., et al., 2014, *J. Chem. Phys.*, 141, 241104
- Petty C., Poirier B., 2014, *Appl. Math.*, 5, 2756
- Polyansky O. L., McKellar A. R. W., 1990, *J. Chem. Phys.*, 92, 4039
- Polyansky O. L., Tennyson J., 1999, *J. Chem. Phys.*, 110, 5056
- Ramanlal J., Tennyson J., 2004, *Mon. Not. R. Astron. Soc.*, 354, 161
- Röhse R., Kutzelnigg W., Jaquet R., Klopper W., 1994, *J. Chem. Phys.*, 101, 2231
- Saito S., Kawaguchi K., Hirota E., 1985, *J. Chem. Phys.*, 82, 45
- Sarka J., Poirier B., 2022, *Front. Phys.*
- Sarka J., Das D., Poirier B., 2021, *AIP Adv.*, 11, 045033
- Sochi T., Tennyson J., 2010, *Mon. Not. R. Astron. Soc.*, 405, 2345
- Stallard T., Miller S., Melin H., Lystrup M., Cowley S. W. H., Bunce E. J., Achilleos N., Dougherty M., 2008a, *Nature*, 453, 1083
- Stallard T., et al., 2008b, *Nature*, 456, 214
- Stark R., van der Tak F. F. S., van Dishoeck E. F., 1999, *Astrophys. J.*, 521, L67
- Tennyson J., Yurchenko S. N., 2012, *Mon. Not. R. Astron. Soc.*, 425, 21
- Tennyson J., Kostin M. A., Barletta P., Harris G. J., Polyansky O. L., Ramanlal J., Zobov N. F., 2004, *Comput. Phys. Commun.*, 163, 85
- Tennyson J., Hill C., Yurchenko S. N., 2013, in 6th international conference on atomic and molecular data and their applications ICAMDATA-2012. AIP, New York, pp 186–195, doi:10.1063/1.4815853
- Tóbiás R., Furtenbacher T., Császár A. G., Naumenko O. V., Tennyson J., Flaud J.-M., Kumard P., Poirier B., 2018, *J. Quant. Spectrosc. Radiat. Transf.*, 208, 152
- Trafton L. M., Geballe T. R., Miller S., Tennyson J., Ballester G. E., 1993, *Astrophys. J.*, 405, 761
- Trafton L. M., Miller S., Geballe T. R., Tennyson J., Ballester G. E., 1999, *Astrophys. J.*, 524, 1059
- Uno T., Kasaba Y., Tao C., Sakanoi T., Kagitani M., Fujisawa S., Kita H., Badman S. V., 2014, *J. Geophys. Res.: Space*, 119, 10,219
- Uy D., Gabrys C. M., Jagod M., Oka T., 1994, *J. Chem. Phys.*, 100, 6267
- Vastel C., Phillips T. G., Yoshida H., 2004, *Astrophys. J.*, 606, L127
- Velilla L., Lepetit B., Aguado A., Beswick J. A., Paniagua M., 2008, *J. Chem. Phys.*, 129, 084307
- Ventrudo B. F., Cassidy D. T., Guo Z. Y., Joo S., Lee S. S., Oka T., 1994, *J. Chem. Phys.*, 100, 6263
- Walmsley C. M., Flower D. R., des Forets G. P., 2004, *Astron. Astrophys.*, 418, 1035
- Warner H. E., Conner W. T., Petrmichl R. H., Woods R. C., 1984, *J. Chem. Phys.*, 81, 2514
- Watson J. K. G., 1984, *J. Mol. Spectrosc.*, 103, 350
- Watson J. K. G., 1994, *Can. J. Phys.*, 72, 702
- Watson J. K. G., et al., 1984, *Can. J. Phys.*, 62, 1875
- Watson J. K. G., Foster S. C., McKellar A. R. W., 1987, *Can. J. Phys.*, 65, 38
- Western C. M., 2017, *J. Quant. Spectrosc. Radiat. Transf.*, 186, 221
- Wu K.-Y., Lien Y.-H., Liao C.-C., Lin Y.-R., Shy J.-T., 2013, *Phys. Rev. A*, 88, 032507
- Xu L., Gabrys C., Oka T., 1990, *J. Chem. Phys.*, 93, 6210
- Xu L. W., Rosslein M., Gabrys C. M., Oka T., 1992, *J. Mol. Spectrosc.*, 153, 726
- Yonezu T., Matsushima F., Moriwaki Y., Takagi K., Amano T., 2009, *J. Mol. Spectrosc.*, 256, 238
- Yu. S., Pearson J. C., Amano T., Matsushima F., 2017, *J. Mol. Spectrosc.*, 331, 6
- Yurchenko S. N., Al-Refaie A. F., Tennyson J., 2018, *Astron. Astrophys.*, 614, A131